

Repository of the Max Delbrück Center for Molecular Medicine (MDC)  
in the Helmholtz Association

<https://edoc.mdc-berlin.de/16915>

**SORLA attenuates EphA4 signaling and amyloid,  $\beta$ -induced  
neurodegeneration**

---

Huang, T.Y., Zhao, Y., Jiang, L.L., Li, X., Liu, Y., Sun, Y., Piña-Crespo, J.C., Zhu, B., Masliah, E., Willnow, T.E., Pasquale, E.B., Xu, H.

This is a copy of the final article, which was originally published in:

Journal of Experimental Medicine  
2017 DEC 04 ; 214(12): 3669-3685  
2017 NOV 07 (first published online)  
doi: [10.1084/jem.20171413](https://doi.org/10.1084/jem.20171413)

Publisher: [Rockefeller University Press](http://www.rupress.org)

Copyright © 2017, Huang et al. This article is distributed under the terms of an Attribution–Noncommercial–Share Alike–No Mirror Sites license for the first six months after the publication date (see <http://www.rupress.org/terms>).



After six months it is available under a Creative Commons License (Attribution–Noncommercial–Share Alike 4.0 International license, as described at <https://creativecommons.org/licenses/by-nc-sa/4.0/>).

# SORLA attenuates EphA4 signaling and amyloid $\beta$ -induced neurodegeneration

Timothy Y. Huang,<sup>1\*</sup> Yingjun Zhao,<sup>1\*</sup> Lu-lin Jiang,<sup>1</sup> Xiaoguang Li,<sup>1</sup> Yan Liu,<sup>1,2</sup> Yu Sun,<sup>1</sup> Juan C. Piña-Crespo,<sup>1</sup> Bing Zhu,<sup>1</sup> Eliezer Masliah,<sup>3,4</sup> Thomas E. Willnow,<sup>5</sup> Elena B. Pasquale,<sup>1,3</sup> and Huaxi Xu<sup>1,2</sup>

<sup>1</sup>Neuroscience Initiative, Sanford Burnham Prebys Medical Discovery Institute, La Jolla, CA

<sup>2</sup>Fujian Provincial Key Laboratory of Neurodegenerative Disease and Aging Research, Institute of Neuroscience, Medical College, Xiamen University, Xiamen, China

<sup>3</sup>Department of Pathology and <sup>4</sup>Department of Neuroscience, University of California, San Diego, La Jolla, CA

<sup>5</sup>Max-Planck-Center for Molecular Medicine, Berlin, Germany

**Sortilin-related receptor with LDLR class A repeats (SORLA, SORL1, or LR11) is a genetic risk factor associated with Alzheimer's disease (AD). Although SORLA is known to regulate trafficking of the amyloid  $\beta$  ( $A\beta$ ) precursor protein to decrease levels of proteotoxic  $A\beta$  oligomers, whether SORLA can counteract synaptic dysfunction induced by  $A\beta$  oligomers remains unclear. Here, we show that SORLA interacts with the EphA4 receptor tyrosine kinase and attenuates ephrinA1 ligand-induced EphA4 clustering and activation to limit downstream effects of EphA4 signaling in neurons. Consistent with these findings, SORLA transgenic mice, compared with WT mice, exhibit decreased EphA4 activation and redistribution to postsynaptic densities, with milder deficits in long-term potentiation and memory induced by  $A\beta$  oligomers. Importantly, we detected elevated levels of active EphA4 in human AD brains, where EphA4 activation is inversely correlated with SORLA/EphA4 association. These results demonstrate a novel role for SORLA as a physiological and pathological EphA4 modulator, which attenuates synaptotoxic EphA4 activation and cognitive impairment associated with  $A\beta$ -induced neurodegeneration in AD.**

## INTRODUCTION

Alzheimer's disease (AD) is a prominent neuropathological disorder that manifests in the age-dependent deposition of extracellular amyloid  $\beta$  ( $A\beta$ ) peptide aggregates at late stages of the disease, whereas soluble  $A\beta$  multimers are thought to exert neurotoxic effects during mild stages of cognitive decline. Synaptic dysfunction occurs at early stages of AD and pathologically correlates with cognitive impairment (Tu et al., 2014; Marttinen et al., 2015). Although familial AD cases are rare, the presence of penetrant AD-associated familial alleles found in the  $A\beta$ -derived amyloid precursor protein (APP) and the APP-cleaving  $\gamma$ -secretase presenilin components (PS1/PS2) supports the importance of  $A\beta$  and APP processing in AD neuropathology (Zhang et al., 2011).

Numerous genetic risk factors have been identified for AD by genome-wide association studies, including class I membrane receptors such as the Sortilin-related receptor with LDLR class A repeats (SORLA; Scherzer et al., 2004; Rogueva et al., 2007). SORLA has been reported to suppress  $A\beta$  generation primarily by trafficking APP away from amyloidogenic cleavage sites, such as the endosome, to the

Golgi (Andersen et al., 2005; Fjorback et al., 2012) and the cell surface (Huang et al., 2016), although other mechanisms may also be involved (Spoelgen et al., 2006; Schmidt et al., 2012). Cellular models have also suggested that SORLA may facilitate  $A\beta$  clearance by binding  $A\beta$  and promoting its trafficking to lysosomes for degradation (Caglayan et al., 2014; Kitago et al., 2015). Recent studies have identified protein coding mutations in late-onset AD (Vardarajan et al., 2015; Louwersheimer et al., 2017), as well as early-onset AD (Potter et al., 2012; Nicolas et al., 2016), giving a strong indication that SORLA dysfunction can enhance the probability of triggering AD onset.

Modulation of SORLA expression in mouse models supports a role in inhibiting APP processing and  $A\beta$  generation. SORLA knockout mouse models show marked elevation in  $A\beta$  levels, whereas SORLA-Rosa26 transgenic overexpression models show significant reduction in  $A\beta$  (Andersen et al., 2005; Caglayan et al., 2014). The connection between SORLA expression levels and  $A\beta$  accumulation is less definitive in human AD brain tissue (Scherzer et al., 2004), suggesting that modifications in SORLA activity or localization also play a role in AD pathogenesis.

There is also evidence that SORLA has additional neuroprotective roles besides promoting anti-amyloidogenic APP

\*T.Y. Huang and Y. Zhao contributed equally to this paper.

Correspondence to Huaxi Xu: xuh@sbnbdiscovery.org

Abbreviations used:  $A\beta$ , amyloid  $\beta$ ; aCSF, artificial cerebrospinal fluid; AD, Alzheimer's disease; ALS, amyotrophic lateral sclerosis; EGF, epidermal growth factor; fEPSP, field excitatory postsynaptic potential; GST, glutathione S-transferase; LTP, long-term potentiation; PSD, postsynaptic density; SORLA, Sortilin-related receptor with LDLR class A repeats; TG, transgenic.



trafficking. In addition to APP, SORLA has been recently shown to bind and regulate the trafficking and signaling of other cell surface receptors, such as the brain-derived neurotrophic factor receptor, TrkB; the glial cell-derived neurotrophic factor receptor, cytokine-like factor 1 (CLF-1); and the insulin receptor (Glerup et al., 2013; Rohe et al., 2013; Larsen et al., 2016; Schmidt et al., 2016). Thus, it is likely that SORLA could also modulate other as-yet-unknown cell surface receptor systems with a role in AD pathogenesis. Indeed, by using a coimmunoprecipitation approach to screen for A $\beta$  cell surface receptors that interact with SORLA, we identified EphA4 (Fu et al., 2014).

EphA4 is a receptor tyrosine kinase with established roles in neuronal wiring and defining cell borders in the developing brain through interaction with ephrin ligands (Pasquale, 2005, 2008; Hruska and Dalva, 2012). In addition, EphA4 remains highly expressed in the adult brain, where it regulates synaptic structure and function (Murai et al., 2003; Carmona et al., 2009; Filosa et al., 2009). More recently, A $\beta$  interaction with EphA4 has been shown to aberrantly activate EphA4, leading to synaptotoxic signals in APP/PS1 mouse models that may involve c-Abl and Cdk5 activation (Fu et al., 2014; Vargas et al., 2014). Here, we demonstrate that SORLA can attenuate EphA4 clustering and activation in response to physiological ephrin ligand stimulation and pathological A $\beta$  oligomers as well as attenuate cognitive memory deficits in mouse models. A late-onset SORLA T947M AD mutation within the EphA4-binding domain of SORLA attenuates EphA4/SORLA interaction and associated EphA4 inactivation. Importantly, decreased SORLA/EphA4 interaction correlates with elevated levels of EphA4 activation via autophosphorylation on Tyr602 in AD patients. Our study reveals a new role for SORLA in suppressing EphA4 activation to ameliorate A $\beta$ -associated synaptotoxicity and cognitive impairment in AD.

## RESULTS

### SORLA interacts with EphA4 and attenuates EphA4 activation

EphB2 and EphA4 are related ephrin receptors that have been recently shown to bind A $\beta$  and mediate its synaptotoxic effects (Cissé et al., 2011; Fu et al., 2014). We therefore investigated whether SORLA can form endogenous complexes with Eph receptors. Analysis of EphA4, EphB1, and EphB2 immunoprecipitates from mouse brain lysates revealed specific coimmunoprecipitation of SORLA with EphA4 (Fig. S1 A). The interaction of SORLA with EphA4 appears similar to that with APP immunoprecipitated from mouse brain lysates (Fig. 1 A). EphA4 and SORLA complexes could also be reconstituted in HEK293 cells. Coexpression of SORLA-glutathione S-transferase (SORLA-GST) with EphA4 and subsequent pull-down with glutathione Sepharose showed association of EphA4 with SORLA-GST, whereas no EphA4 association was observed with GST alone (Fig. 1 B). In addition, an EphA4-Fc fusion protein comprising the EphA4

ectodomain immobilized on protein G Sepharose could pull down SORLA from cell lysates (Fig. S1 B).

Its interaction with EphA4 suggests that SORLA could be an EphA4 substrate. To examine this, we overexpressed EphA4 WT or the kinase-dead K653R mutant in HEK293 cells and examined SORLA and EphA4 immunoprecipitates for tyrosine phosphorylation (Fig. S1 C). We observed phosphorylation of EphA4 WT but not the K653R mutant, as expected. However, we did not detect SORLA tyrosine phosphorylation (Fig. S1 C), suggesting that the short cytoplasmic portion of SORLA is not a substrate for EphA4.

We next considered the possibility that SORLA influences EphA4 activation in response to ephrin ligand (ephrinA1-Fc) stimulation. Using HEK293 cells stably expressing EphA4 (HEK-A4), we observed rapid ephrinA1-Fc-induced EphA4 phosphorylation on Y602 indicative of activation, which persisted for several hours (Fig. S1 D). Similar EphA4 activation was also observed in WT cortical neurons (Fig. S1 E). Interestingly, overexpression of SORLA in HEK-A4 cells attenuated EphA4 activation in response to ephrinA1-Fc stimulation (Fig. 1, C and D). Similarly, EphA4 activation induced by ephrinA1-Fc was lower in cortical neurons derived from SORLA transgenic (TG) mice compared with WT neurons (Fig. 1 E), whereas basal EphA4 activation in WT and SORLA TG neurons was not significantly different (Fig. S1 F). Conversely, neuronal cultures derived from SORLA KO mice exhibited enhanced EphA4 activation in response to ephrinA1-Fc stimulation compared with WT neurons (Fig. S1 G). Together, these results demonstrate a novel interaction between SORLA and EphA4 and suggest that SORLA is a negative modulator of EphA4 activation.

### SORLA attenuates ephrin ligand-induced growth cone collapse

Ephrin-induced EphA4 activation in neurons triggers the activation of RhoGTPase-mediated actin cytoskeleton rearrangements, leading to growth cone collapse, which is critical for axon guidance during development (Shamah et al., 2001; Shi et al., 2007). To examine whether modulating SORLA levels could alter physiological responses mediated by EphA4 signaling, we cultured hippocampal neurons derived from WT, SORLA TG, or SORLA KO mice and determined the effects of SORLA levels on ephrinA1-Fc-induced growth cone collapse. After 3 d in culture, WT neurons featured F-actin-rich growth cones at the tip of long axonal processes (Fig. 2, A and B). WT, SORLA TG, or SORLA KO neurons from several independent embryonic dissections were stimulated with ephrinA1-Fc, or Fc as a control, and fluorescently labeled growth cones were scored as collapsed or not collapsed. In agreement with previous studies (Egea et al., 2005; Richter et al., 2007; Shi et al., 2007; Fu et al., 2014), 82% of the WT growth cones were collapsed after 30 min of ephrinA1-Fc stimulation, representing a threefold increase compared with Fc control stimulation (Fig. 2, A, C, and D). SORLA TG growth cones were less responsive, with

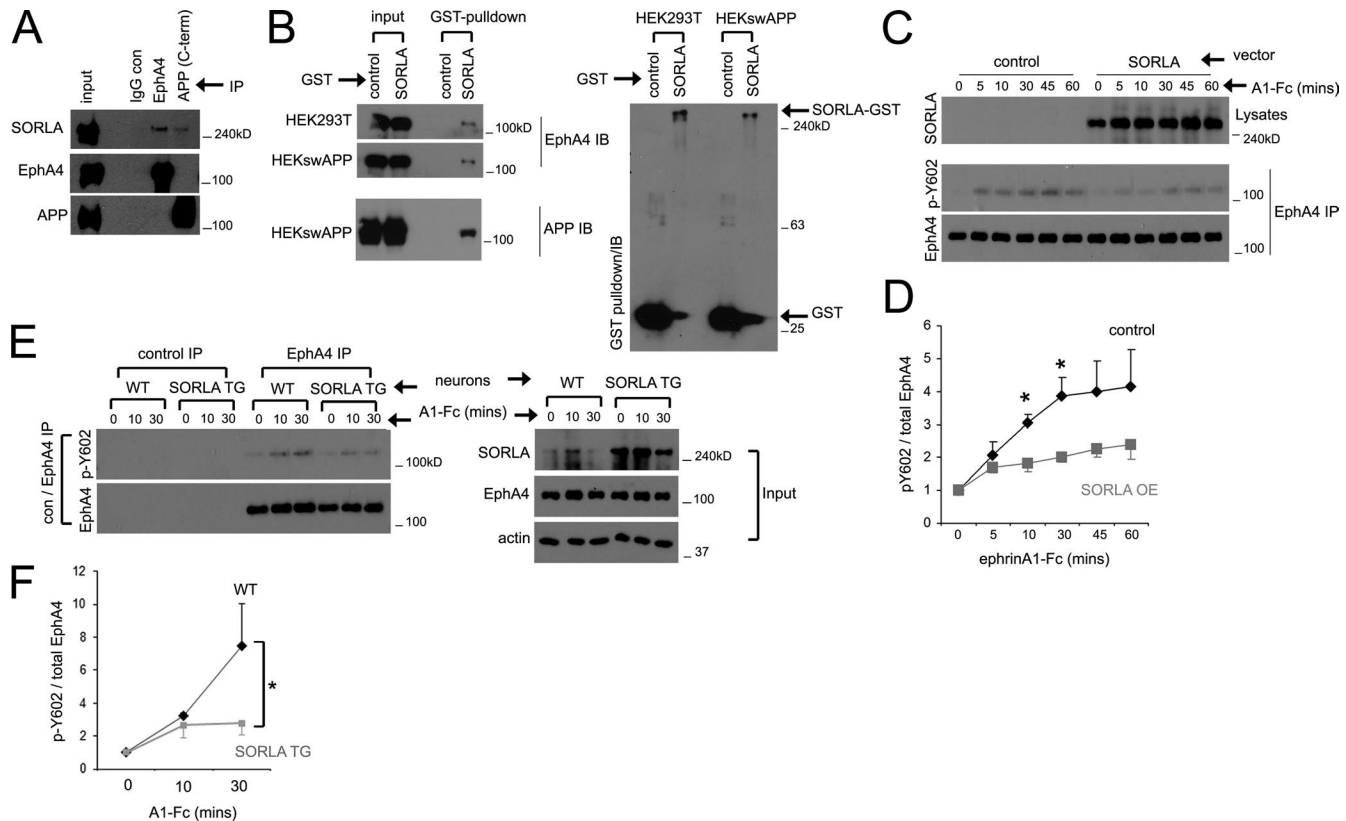


**Figure 1. SORLA interacts with EphA4 and suppresses EphA4 activation in response to ligand stimulation.** (A) SORLA coimmunoprecipitates with EphA4. EphA4 or APP was immunoprecipitated with the indicated antibodies and immunoblotted for SORLA, EphA4, or APP. (B) SORLA/EphA4 complexes can be reconstituted by exogenous expression. EphA4 was coexpressed with GST or SORLA-GST in HEK293T or HEKswAPP cell lines, and glutathione Sepharose precipitates were immunoblotted for EphA4, APP (left), or GST (right). A single representative experiment is shown in A and B. (C–E) SORLA overexpression attenuates EphA4 activation. (C) HEK293 cells stably expressing EphA4 were transfected with control or SORLA constructs and incubated with ephrinA1-Fc (A1-Fc) for the time indicated. EphA4 immunoprecipitates were immunoblotted for pY602 phosphorylation or total EphA4. Data in D represents mean  $\pm$  SE from five independent experiments (\*,  $P < 0.05$ ; Student's *t* test). (E) WT or SORLA-overexpressing transgenic (SORLA TG) cortical neurons were stimulated with ephrinA1-Fc, and control or EphA4 immunoprecipitates were immunoblotted for EphA4 pY602 or total EphA4 as indicated. Lysate inputs are shown (right). (F) Cumulative data from E; graphs represent mean  $\pm$  SE from seven independent experiments (\*,  $P < 0.05$ ; Student's *t* test).

only 48% of the growth cones scored as collapsed after ephrinA1-Fc stimulation (representing a 1.5-fold increase over Fc-treated controls) and numerous neurons retaining intact growth cones (52%; Fig. 2, B–D). Interestingly, SORLA KO neurons exhibited high basal growth cone collapse (Fc treatment; Fig. 2 C), and most growth cones were collapsed after ephrinA1-Fc stimulation (Fig. 2 C). Together, these results support a role for SORLA in suppressing ephrin-induced EphA4 signaling activities.

#### SORLA attenuates ephrin ligand-induced EphA4 clustering

As a regulator of protein trafficking, SORLA has been shown to modulate the cell surface localization of receptors such as TrkB and the insulin receptor (Rohe et al., 2013; Schmidt et al., 2016). However, we did not observe changes in EphA4 cell surface levels in HEK293T cells and neurons overexpressing SORLA (Fig. S2 A), SORLA TG neurons (Fig. S2 C), SORLA siRNA knockdown HEK293T cells, or SORLA

KO neurons (Fig. S2 B). Biochemical fractionation also did not reveal a significant difference in EphA4 distribution in Triton X-100-soluble and -insoluble postsynaptic density (PSD) membrane fractions in WT and SORLA TG mice (Fig. S2, D and E).

Interestingly, SORLA interaction with APP has been previously shown to inhibit APP oligomerization (Schmidt et al., 2012). Because ligand-mediated EphA4 homotypic clustering precedes EphA4 activation (Egea et al., 2005), we hypothesized that SORLA may inhibit EphA4 activation by interfering with receptor clustering. We observed formation of endogenous EphA4 clusters in noncollapsed hippocampal growth cones after short-term ephrinA1-Fc stimulation (5 min), whereas more prolonged ephrinA1-Fc stimulation (30 min) produced EphA4 clusters in collapsed growth cones (Fig. 3 A). Comparison of EphA4 immunoreactivity in WT, SORLA TG, and SORLA KO neurons stimulated with ephrinA1-Fc for 5 min suggested the preferential formation of

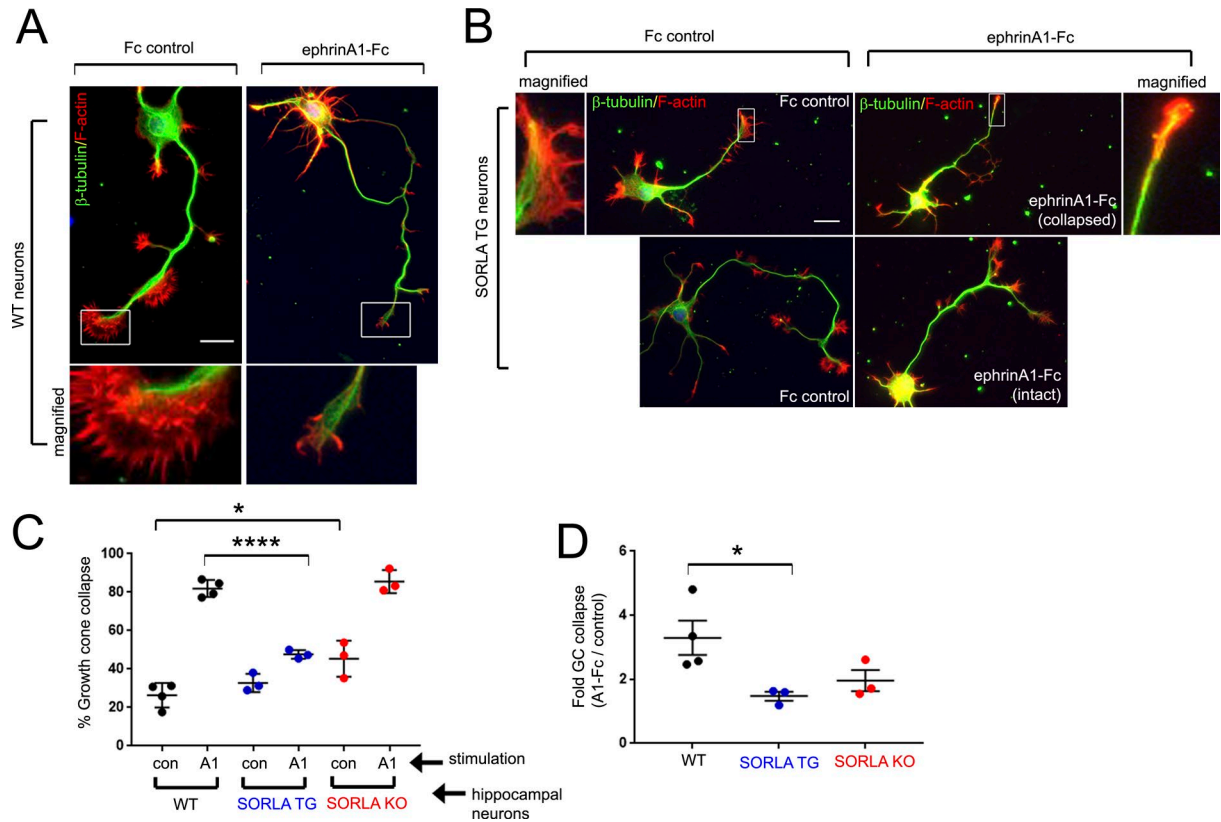


**Figure 2. SORLA overexpression attenuates ephrin-mediated growth cone collapse.** (A and B) Characterization of ephrinA1-mediated growth cone collapse in hippocampal neurons. WT (A) or SORLA TG (B) hippocampal neurons were treated with Fc control or ephrinA1-Fc for 30 min at DIV3 and stained for tubulin (green) and F-actin (red). Boxed regions are magnified as indicated. Bars, 10  $\mu$ m. (C and D) Evaluation of growth cone collapse in WT, transgenic SORLA (TG) or knockout (KO) hippocampal neurons. (C) WT, SORLA TG, and KO hippocampal neurons were treated with Fc or ephrinA1-Fc for 30 min and stained for F-actin and tubulin. Growth cones at the tips of axonal processes were imaged and scored into collapsed and noncollapsed categories. The percentage of growth cone collapse was calculated in a minimum of three independent dissections, with each data point in the graph representing a separate dissection. (D) Fold growth cone (GC) collapse observed with ephrinA1-Fc treatment over Fc control for WT, TG, or KO neurons calculated for each experiment in C. In C and D, graphs represent mean  $\pm$  SE; \*,  $P < 0.05$ ; \*\*\*\*,  $P < 0.00001$ ; Student's  $t$  test.

EphA4 clusters in WT and SORLA KO neurons, with few clusters observed in SORLA TG neurons (Fig. 3 B). We therefore measured EphA4 cluster formation in F-actin-labeled growth cones stimulated with ephrinA1-Fc for 5 min, which revealed a significantly attenuated EphA4 clustering response in SORLA TG neurons and a slightly enhanced EphA4 clustering response in SORLA KO neurons (Fig. 3, C and D). Because we did not observe any differences in overall EphA4 labeling intensity in WT, SORLA TG, or SORLA KO growth cones (Fig. 3 E), SORLA does not appear to affect aggregation through changes in EphA4 levels, consistent with the immunoblotting data shown in Fig. S2 C. These results demonstrate that SORLA inhibits EphA4 activation by decreasing ephrin-induced EphA4 clustering. Although our results suggest that SORLA does not affect cell surface distribution of EphA4 at steady state, it remains possible that SORLA may affect EphA4 trafficking with ligand stimulation, likely through attenuating EphA4 clustering kinetics with ligand stimulation.

### An AD-associated mutation in the SORLA YWTD/epidermal growth factor (EGF)-like region impairs SORLA/EphA4 interaction

Because SORLA interacts with the extracellular region of EphA4 (Fig. S1 B), we hypothesized that the extracellular region of SORLA mediates the interaction with EphA4. The large SORLA extracellular region includes an N-terminal VPS10 domain, a YWTD/EGF-like region, multiple LDLR class A repeats, and multiple fibronectin type III repeats (Fig. 4 A). To identify the SORLA domains that interact with EphA4, we purified full-length EphA4 containing C-terminal FLAG and hexahistidine tags (EphA4-FLAGhis6) from HEK293 cells (Fig. S3 A) and measured its association with Fc fusion proteins of various SORLA extracellular fragments immobilized on protein G Sepharose (Fig. 4 B). This process revealed an interaction between EphA4 and the SORLA YWTD/EGF-like region, indicating a critical role for this region of SORLA in mediating the association with EphA4.

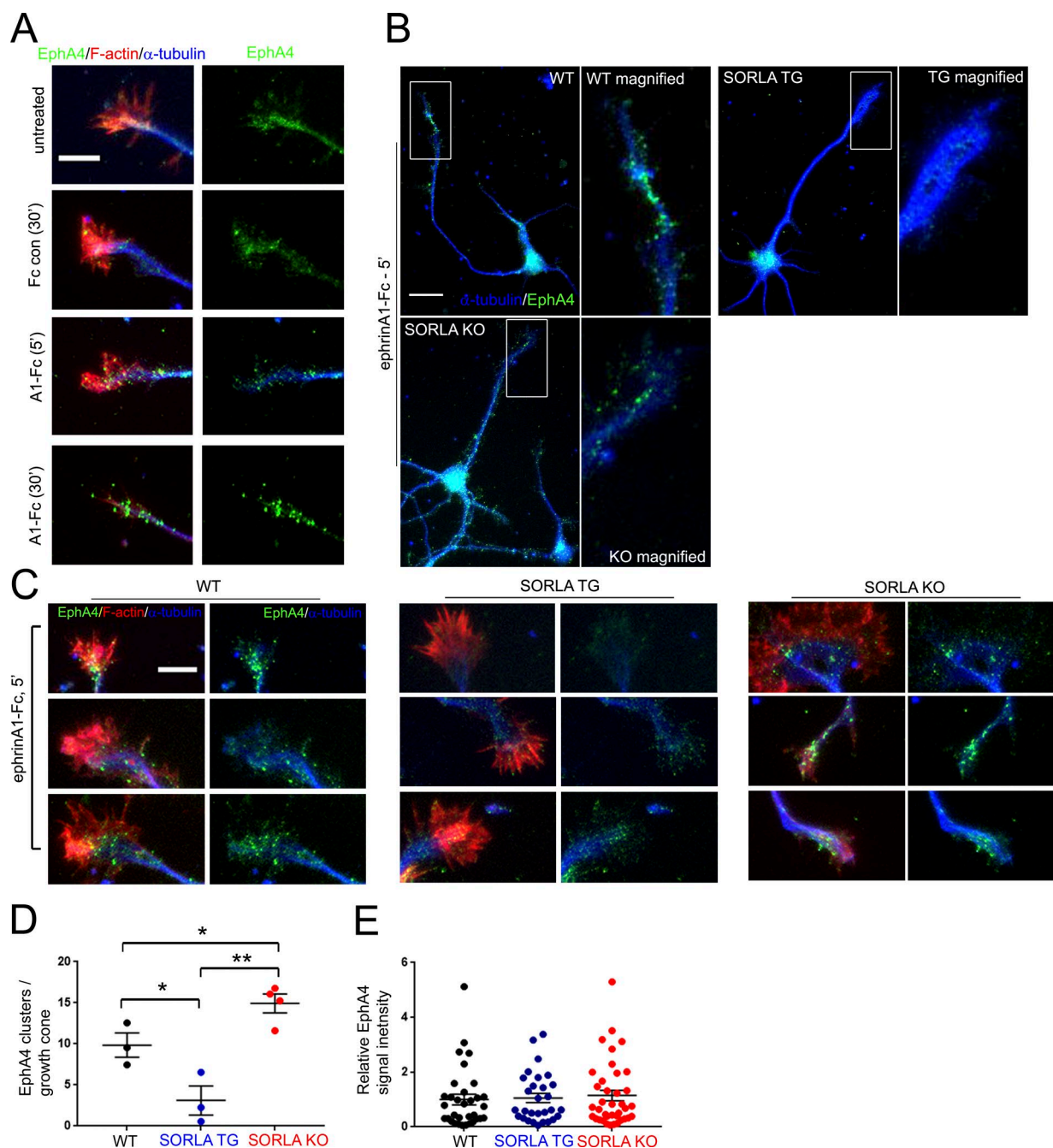


**Figure 3. SORLA overexpression attenuates ephrinA1-induced EphA4 clustering.** (A) WT hippocampal neurons at DIV3, untreated or exposed to control Fc for 30 min or ephrinA1-Fc for the indicated time, were fixed and stained for EphA4 (green), F-actin (red), or tubulin (blue). Note that ephrinA1-Fc treatment for 5 min results in EphA4 clustering without growth cone collapse. Bar, 5  $\mu$ m. (B–D) Evaluation of EphA4 clustering in WT, SORLA TG, and KO hippocampal neurons. (B) WT, SORLA TG, and KO hippocampal neurons were treated with ephrinA1-Fc for 5 min and stained for EphA4 (green) and tubulin (blue). Boxed regions are magnified in the adjacent panels. Bar, 10  $\mu$ m. (C) EphA4 clustering within F-actin-rich areas was examined by microscopy in WT, SORLA TG, and SORLA KO hippocampal neurons at DIV3 by staining for EphA4 (green), F-actin (red), and tubulin (blue). Bar, 5  $\mu$ m. EphA4 clusters  $\geq 200$  nm within F-actin-enriched growth cone regions were scored in a minimum of four independent dissections/experiments (D); graph represents mean  $\pm$  SE, from individual experiments; \*,  $P < 0.05$ ; \*\*,  $P < 0.003$ ; Student's *t* test. (E) Total EphA4 fluorescence intensities from individual growth cones scored in D were plotted; graph represents mean  $\pm$  SE.

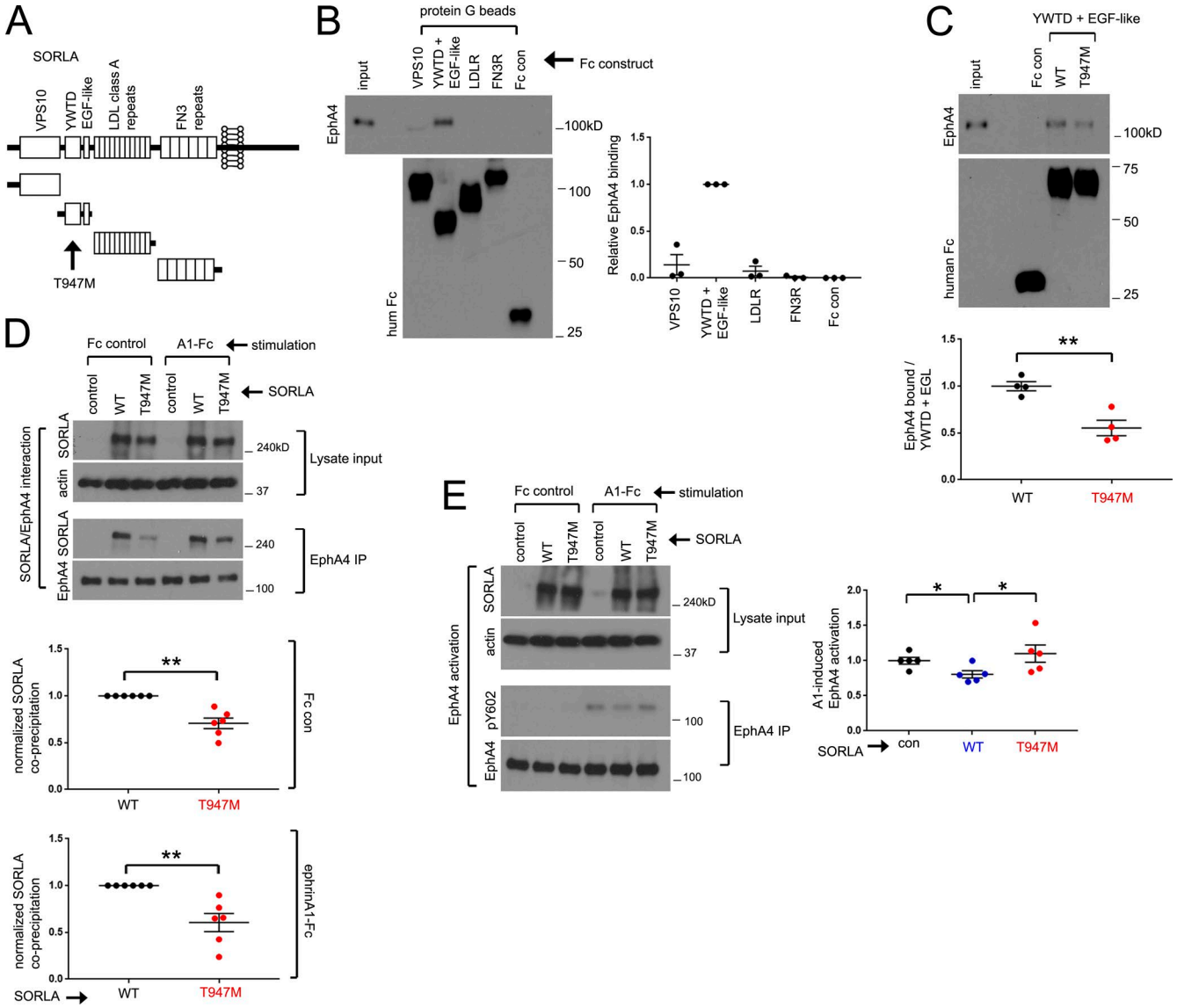


**Figure 4. EphA4 interacts with the SORLA YWTD/EGF-like domain, and EphA4/SORLA interaction is attenuated by a T947M AD-associated SORLA mutation.** (A) Schematic diagram of SORLA domains; an AD-associated T947M mutation resides within the YWTD/EGF-like region. (B) The SORLA YWTD/EGF-like region interacts with EphA4. Purified EphA4-FLAGhis6 was incubated with various SORLA domain-Fc fusion proteins immobilized on protein G Sepharose, and coprecipitation with EphA4 was evaluated by immunoblotting. Adjacent graph depicts relative EphA4 coprecipitation (YWTD/EGF set to 1.0). Results are from three independent experiments; graph represents mean  $\pm$  SE. (C) Purified EphA4 was evaluated for coprecipitation with WT or a T947M variant of the SORLA YWTD/EGF domain fused to Fc as in B. The adjacent graph depicts relative EphA4 binding with the WT construct set to 1.0 in four replicates from two independent experiments, mean  $\pm$  SE; \*\*,  $P < 0.005$ ; Student's *t* test. (D and E) The SORLA T947M mutation attenuates SORLA/EphA4 interaction and effects on EphA4 activation. HEK293 cells stably expressing EphA4 were transfected with control, WT, or T947M SORLA expression constructs, and EphA4 immunoprecipitates from lysates were evaluated for SORLA coprecipitation (D) or ephrinA1-Fc induced EphA4 activation (E) by immunoblotting. Graphs in D depict T947M coprecipitation relative to WT (set to 1.0; mean  $\pm$  SE; \*\*,  $P < 0.005$ ; Student's *t* test) from six replicates in four independent experiments. Graphs in E show relative pY602/EphA4 ratios with control vector treatments set to 1.0 (mean  $\pm$  SE from five replicates in three independent experiments; \*,  $P < 0.015$ ; paired Student's *t* test).

Interestingly, a SORLA T947M variant within the YWTD/EGF-like region (Fig. 4 A) was identified in late-onset AD patients and segregated with AD onset in some familial lineages analyzed (Vardarajan et al., 2015). Coprecipitation of purified EphA4-FLAGhis6 with the SORLA

WT or T947M variant YWTD/EGF-like domain fused to Fc revealed weaker interaction of the T947M variant domain with EphA4 (Fig. 4 C). Analysis of EphA4 immunoprecipitates from HEK-A4 cells transfected with full-length SORLA WT or the T947M variant revealed that the T947M muta-

tion also impairs association with EphA4 in the context of full-length SORLA, with or without ephrinA1-Fc stimulation (Fig. 4 D). In addition, the SORLA T947M variant was less effective than SORLA WT in inhibiting ephrinA1-Fc-induced EphA4 activation (Fig. 4 E).

### SORLA attenuates A $\beta$ -mediated EphA4 activation and clustering

We found that EphA4 immunoprecipitates from SORLA TG mouse hippocampus show a slight reduction in EphA4 activation compared with WT hippocampus (Fig. 5, A and B), suggesting that SORLA suppresses EphA4 activation by ephrin ligands not only in cultured neurons but also *in vivo*. Previous studies indicated a role for EphA4 signaling in mediating the synaptotoxic effects of A $\beta$  oligomers (Fu et al., 2014; Vargas et al., 2014). Given that SORLA can attenuate EphA4 activation in response to physiological ephrin stimulation, we investigated whether SORLA can likewise suppress EphA4 activation and clustering in response to A $\beta$  oligomers. We therefore oligomerized A $\beta$  (A $\beta$ <sub>1-42</sub>; Fig. 5 C), exposed WT and SORLA TG cortical neurons to the A $\beta$  oligomers, and evaluated EphA4 immunoprecipitates for EphA4 activation by immunoblotting (Fig. 5, D and E). Remarkably, A $\beta$  treatment caused a nearly twofold increase in EphA4 activation in WT neurons but not in SORLA TG neurons (Fig. 5, D and E). Similar to ephrinA1-Fc stimulation, we also observed EphA4 clustering in HEK293T cells treated with A $\beta$  oligomers (Fig. S3 B), and SORLA overexpressed together with GFP as a marker largely attenuated A $\beta$ -induced EphA4 cluster formation compared with GFP alone in control cells (Fig. S3 C). These results indicate that SORLA can impair EphA4 activation not only in response to ephrin stimulation but also in response to pathological stimulation by A $\beta$  oligomers.

### SORLA ameliorates A $\beta$ -induced cognitive impairment as well as associated EphA4 activation and redistribution to PSDs

EphA4 activation and synaptic redistribution induced by exposure to A $\beta$  oligomers have been previously shown to cause synaptotoxic effects (Fu et al., 2014; Vargas et al., 2014). Therefore, we investigated whether SORLA-mediated inhibition of EphA4 activation could ameliorate the detrimental effects of A $\beta$  oligomers on spatial learning and memory tasks by examining WT and SORLA TG mice in the Morris water maze test. Because SORLA may influence A $\beta$  levels in mouse AD models, we stereotactically injected human A $\beta$  oligomers into the WT and SORLA TG mouse hippocampus and measured spatial learning and memory 1 wk after injection.

In agreement with our previous analyses using the Morris water maze test (Yan et al., 2016), hippocampal injection of A $\beta$  oligomers impaired cognitive spatial learning capacity in WT mice during consecutive platform training sessions (Fig. 5 F). In contrast, SORLA TG animals were resistant to the effects of A $\beta$  throughout the period of platform training. After platform training, the mice were assessed for their

ability to return to the platform area in the water maze. The WT mice injected with A $\beta$  oligomers exhibited significant impairment in finding the platform, whereas A $\beta$ -injected SORLA TG mice performed as well as WT and SORLA TG mice injected with PBS as a control (Fig. 5 G).

The mice were killed immediately after behavioral testing, and immunoblot analyses of EphA4 immunoprecipitates from total hippocampal synaptosome fractions revealed significantly increased EphA4 activation in WT mice injected with A $\beta$  oligomers compared with PBS-injected control mice (Fig. 5 H), whereas A $\beta$ -injected SORLA TG mice did not show increased EphA4 activation (Fig. 5 I). Measurement of human A $\beta$  after behavioral analysis confirmed that A $\beta$  levels were the same in A $\beta$ -injected WT and SORLA TG mice (Fig. S3 D). We further used confocal microscopy to examine histological sections from WT and SORLA TG mice injected in the hippocampal region with A $\beta$  oligomers or PBS to investigate possible changes in the colocalization of EphA4 with PSD95 in the dentate gyrus (Fig. 6, A and B). We detected more puncta labeled for both EphA4 and PSD95 in WT hippocampal sections from mice injected with A $\beta$  oligomers compared with PBS controls, but not in SORLA TG sections (Fig. 6, B and C).

Consistent with previous studies showing long-term potentiation (LTP) defects with hippocampal A $\beta$  oligomer (Yan et al., 2016) or AAV-APP/PS1 injection (Audrain et al., 2016), we also observed a reduction in LTP in WT hippocampal slices treated with A $\beta$  oligomers, whereas SORLA TG hippocampal slices were resistant to A $\beta$ -mediated LTP impairment (Fig. 6, D–F). Thus, SORLA can suppress postsynaptic dysfunction induced by A $\beta$  oligomers, which has been previously linked to aberrant EphA4 activation by A $\beta$  oligomers (Fu et al., 2014; Vargas et al., 2014). Together, these results indicate that up-regulation of SORLA can suppress cognitive deficiencies associated with EphA4 activation/redistribution phenotypes and electrophysiological LTP impairment resulting from exposure to A $\beta$  oligomers.

### Elevated EphA4 activation in human AD brain tissue correlates with reduced SORLA/EphA4 association

Our data in cell culture and in mice support a model in which SORLA interacts with EphA4 to attenuate A $\beta$ -dependent EphA4 activation and cognitive impairment (Fig. S4 A). To verify the validity of this model in human AD patients, we used 30 AD and 23 control brain tissue samples from human frontal cortex regions (Table S1) to prepare lysates and synaptosomes for immunoblotting and EphA4 immunoprecipitation analyses. We did not observe any significant change in SORLA or EphA4 levels between our AD and control cohorts (Fig. 7 A and Fig. S4, B and C). However, EphA4 activation was significantly higher in brain tissue from the AD patients than the controls (Fig. 7, B and C; and Fig. S4 B). Furthermore, no significant overall difference in SORLA/EphA4 association was observed between AD and control patients (Fig. S4 D). Because variations in both EphA4 activa-

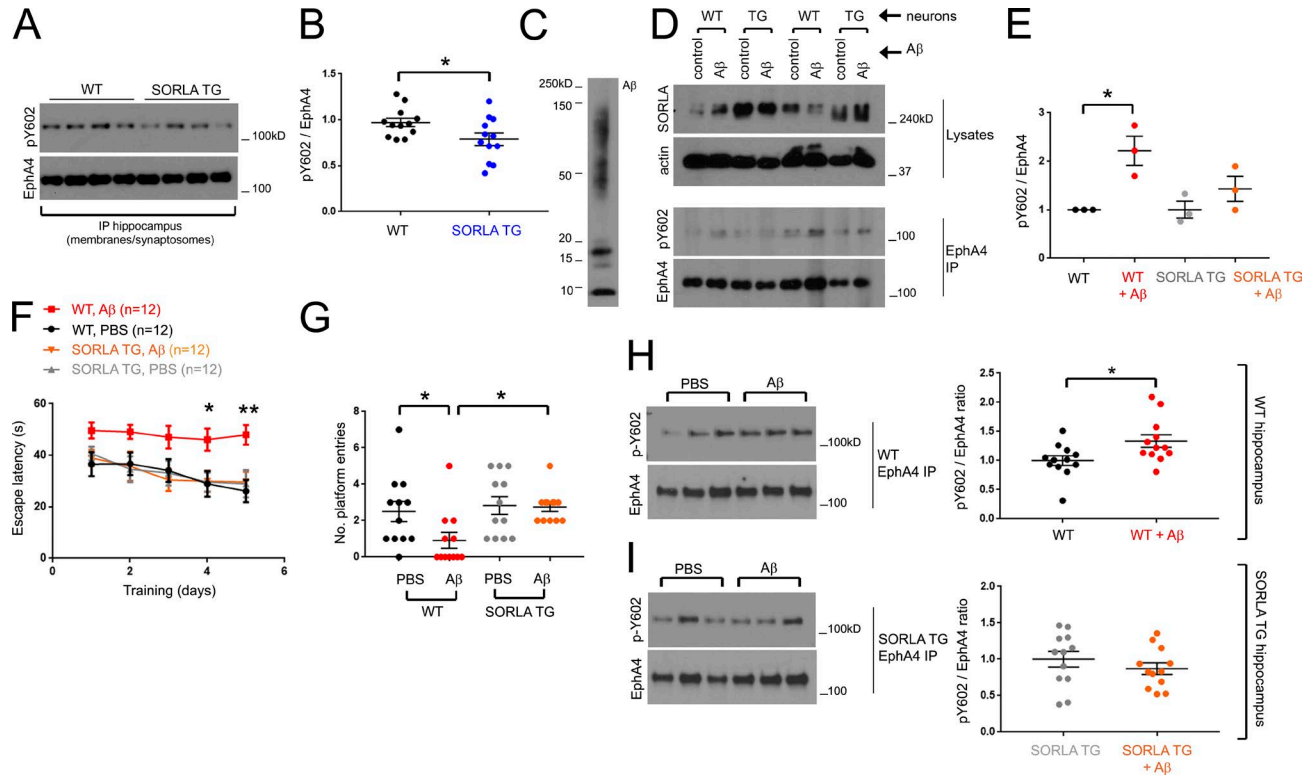


**Figure 5. SORLA suppresses Aβ-mediated EphA4 activation and attenuates cognitive and synaptotoxic deficits associated with oligomeric Aβ injection in SORLA TG mice.** (A and B) SORLA TG mice show a slight reduction in EphA4 activation at steady state. (A) EphA4 immunoprecipitates from crude synaptosome fractions in 3-mo-old WT and SORLA TG mice were subjected to immunoblotting, and pY602/EphA4 ratios were plotted in B. Graph represents mean ± SE from WT, *n* = 12, and SORLA TG, *n* = 12 animals (\*, *P* < 0.04; Student's *t* test). (C–E) SORLA suppresses Aβ-mediated EphA4 activation. Aβ<sub>1–42</sub> oligomers (C) were applied to WT or SORLA TG cortical neurons for 2 h, and Eph4 immunoprecipitates (D) were evaluated for EphA4 activation. (E) Relative fold pY602/EphA4 ratios were evaluated for WT and SORLA TG (TG) neurons (graphs depict mean ± SE from three replicates from two independent experiments; \*, *P* < 0.04; Student's *t* test). (F and G) SORLA suppresses spatial memory deficits associated with hippocampal Aβ injection. WT and SORLA TG mice (*n* = 12, each group; *n* = 48 total, two independent assay runs) were stereotactically injected with PBS or Aβ into the hippocampus and subjected to 5 d of navigational training to find a hidden platform. (F) Escape latency decreased for all groups except WT Aβ-injected animals (red). Graph represents mean ± SE (\*, *P* < 0.03; \*\*, *P* < 0.008; two-way ANOVA). (G) After training, a probe test was performed to determine whether animals could accurately recall and return to the platform area; the number of entries was automatically recorded for the experimental groups. Significance was determined using one-way ANOVA (mean ± SE; \*, *P* < 0.05). (H and I) SORLA attenuates Aβ-mediated EphA4 activation. Hippocampal tissue from WT (H) and SORLA TG (I) mice injected with PBS or Aβ were subjected to biochemical fractionation after behavioral analysis, and EphA4 immunoprecipitates from membranes/total synaptosomes were immunoblotted for activated EphA4 (pY602) and total EphA4. pY602/EphA4 ratios were normalized to PBS injected samples (set to 1.0). Graphs represent mean ± SE; \*, *P* < 0.05; Student's *t* test.

tion and EphA4/SORLA association were observed in both control and AD patients (Fig. 7 C and Fig. S4 D), we examined whether there may be a correlation between the two parameters (Fig. 7 D). Interestingly, we observed a significant inverse correlation between SORLA/EphA4 association and EphA4 activation in AD patients by linear regression analysis (Fig. 7 D), implying that SORLA/EphA4 association correlates with attenuated EphA4 activation in AD brain tissue. This may represent a critical mechanism that could be fundamental for neuroprotection, particularly at earlier stages of cognitive decline.

**DISCUSSION**

The complexity of AD as a neurological disorder is a key impediment in the search for effective drug targets to treat

or reverse AD-associated cognitive decline. Current targeting strategies mainly focus on inhibiting the generation or promoting the clearance of Aβ in its various forms (Lukiw, 2012). Although these strategies may be beneficial against AD, no drug developed so far has demonstrated clinical efficacy.

SORLA represents a unique target for consideration. As an AD risk factor, SORLA has been traditionally classified as an upstream regulator of Aβ homeostasis, which may act to suppress amyloidogenic cleavage pathways by regulating APP trafficking (Andersen et al., 2005; Fjorback et al., 2012; Huang et al., 2016), APP oligomerization (Schmidt et al., 2012), and Aβ clearance (Caglayan et al., 2014). Here, we present new evidence that SORLA also acts downstream of Aβ to attenuate neurotoxicity through the modulation of Aβ

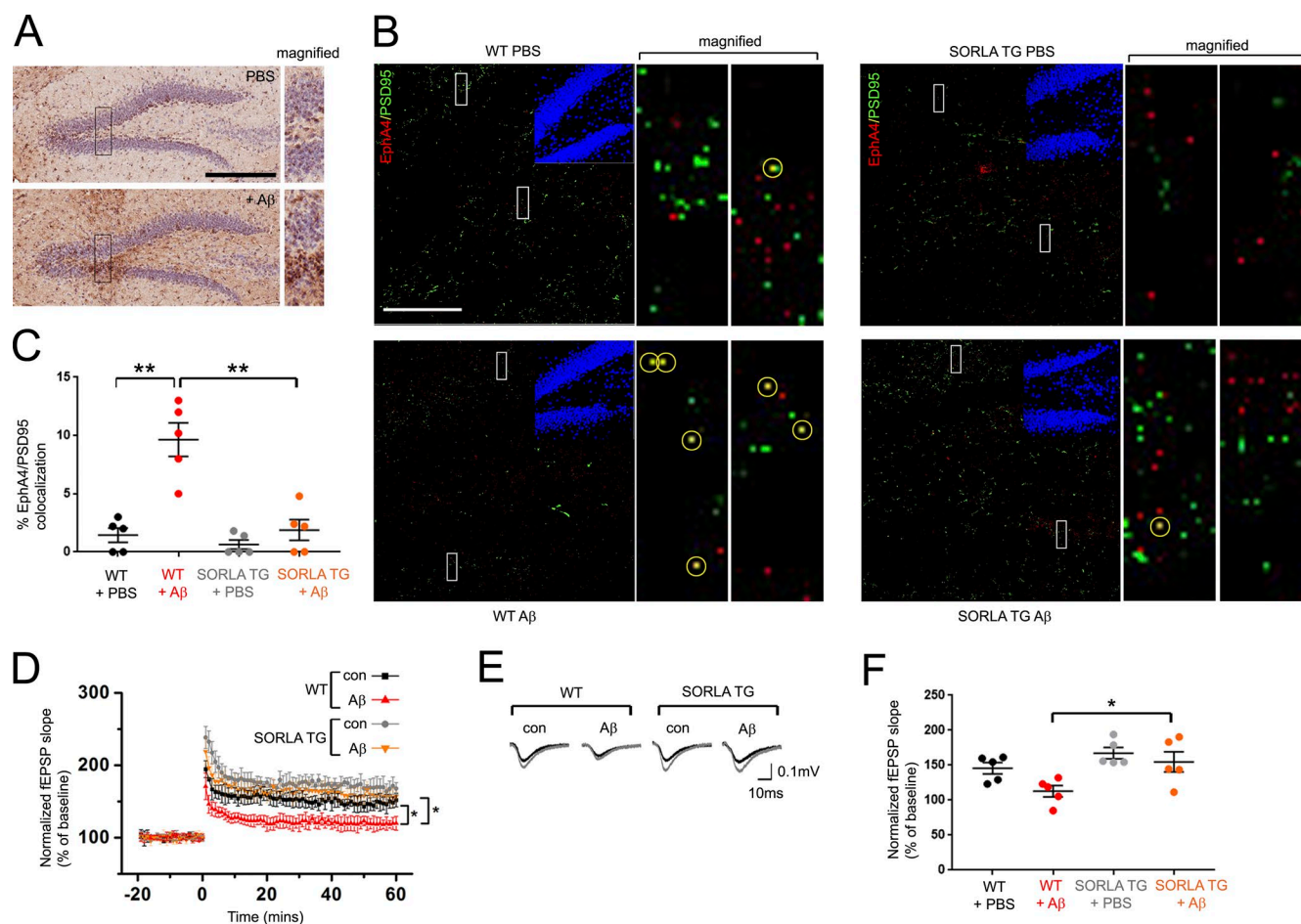


**Figure 6. EphA4 redistribution to PSD clusters and LTP impairment is attenuated in SORLA TG mice.** (A and B) Hippocampal A $\beta$  injection induces EphA4 redistribution to PSD95 puncta. WT and SORLA TG mice were injected with PBS or A $\beta$  and subjected to immunohistological staining for A $\beta$  (brown) using MOAB-2 antibody (A) or costaining for EphA4 (red) and PSD95 (green); B. DAPI (blue) insets in B depict the dentate gyrus region imaged. Bars: (A) 300  $\mu$ m; (B) 100  $\mu$ m. Boxes in A and B are magnified in adjacent panels. EphA4/PSD95 co-staining puncta (yellow) are marked by yellow circles in magnified panels in B. (C) Graph indicates percentage of red/green overlapping puncta scored for five 100- $\mu$ m-square regions from hippocampal sections (mean  $\pm$  SE; \*\*,  $P < 0.001$ ; Student's  $t$  test). (D and E) SORLA overexpression restores A $\beta$ -induced LTP impairment. Mean fEPSP slopes normalized over baseline values are shown for WT and SORLA TG acute slices under steady-state conditions with or without 500 nM A $\beta$  as indicated. Baseline recordings were taken 20 min before LTP induction (0 time point), and 60 min after LTP induction. Graph represents mean  $\pm$  SE; \*,  $P < 0.05$ . (E) Representative fEPSP recordings obtained before (black) and after (gray) high-frequency stimulation. (F) Cumulative fEPSP slopes between 50 and 60 min after LTP induction (mean  $\pm$  SE,  $\geq 5$  slices per mouse/three mice per genotype/treatment category). Statistical values were calculated using two-way ANOVA; \*,  $P < 0.05$ .

receptors such as EphA4, hence affecting synaptic function. Should SORLA affect both means of A $\beta$ -associated neuroprotection concurrently, neurological function could be sensitive to subtle alterations in SORLA levels or function.

Ephrin receptors such as EphA4 are important early in brain development and mediate fundamental processes including axon guidance and synaptic wiring (Pasquale, 2005, 2008; Hruska and Dalva, 2012). EphA4 is also highly expressed in adult brain and has important functions in synaptic structure and function (Murai et al., 2003; Carmona et al., 2009; Filosa et al., 2009). In addition, it is becoming apparent that EphA4 plays a role in the pathogenesis of neurological disorders such as AD and amyotrophic lateral sclerosis (ALS). So far, it is

unclear whether definitive changes in total EphA4 levels are altered in AD: although SNPs have been identified proximal to the EphA4 gene locus in late onset AD cohorts (Shen et al., 2010), studies have revealed either no change (Rosenberger et al., 2014) or slight reductions in EphA4 expression in the brain of AD patients (Simón et al., 2009). Interestingly, however, EphA4 immunoreactivity has been observed in human AD brain near A $\beta$  plaques (Rosenberger et al., 2014). Because A $\beta$  oligomers can induce EphA4 clustering at PSD-bearing spines (Fu et al., 2014), these pathological EphA4/A $\beta$  plaque aggregates may be remnant pathological byproducts formed by prolonged A $\beta$ -induced EphA4 aggregation. Our results demonstrate that EphA4 is also aberrantly activated in human

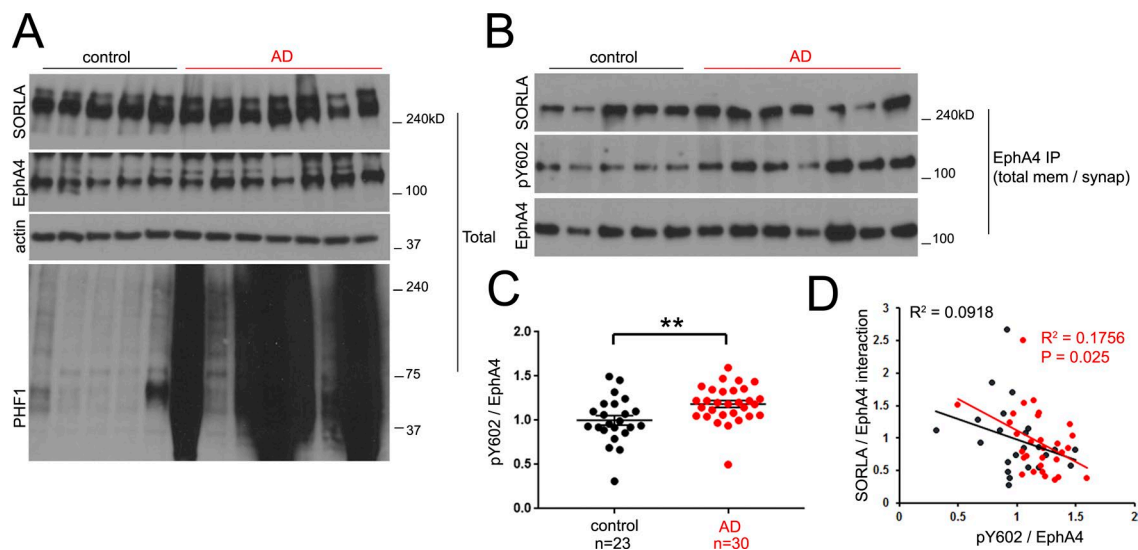


**Figure 7. EphA4 activation is observed in human AD and correlates with decreased EphA4/SORLA interaction.** (A) Total lysates were generated from a representative control and AD cohort and immunoblotted with the indicated antibodies. (B and C) Elevated EphA4 activity is observed in AD. (B) EphA4 was immunoprecipitated from total synaptosome fractions generated from human frontal cortex and immunoblotted for activated EphA4, pY602, or SORLA as indicated. (C) Activated EphA4 (pY602/EphA4 ratios) as determined in B were plotted for control ( $n = 23$ ) and AD ( $n = 30$ ) patient cases. Graph represents mean  $\pm$  SE (\*\*,  $P < 0.02$ ; Student's  $t$  test). (D) Enhanced SORLA/EphA4 interaction correlates with attenuated EphA4 activation. SORLA/EphA4 and pY602/EphA4 ratios were individually plotted for control (black) and AD (red) patients.  $R^2$  (goodness of fit) values are shown for control (black) and AD (red) data groups; the  $p$ -value (significant deviance of the slope from 0 by linear regression analysis) for the AD group was found to be significant.

AD brain tissue. Because  $A\beta$ -mediated EphA4 activation results in synaptotoxicity that can be reversed by pharmacological EphA4 inhibitors (Fu et al., 2014; Vargas et al., 2014), it is likely that EphA4 may contribute to synaptic deficiencies that accompany cognitive decline in AD.

Given that aberrant EphA4 activation is apparent in AD, it is possible that downstream EphA4 pathways are likewise affected. EphA4 was previously found to recruit and activate Cdk5 with ephrin ligand stimulation (Fu et al., 2007). Interestingly, Cdk5 activity and its activators were also found to be elevated in human AD brain compared with controls (Lee et al., 1999; Tseng et al., 2002). Collectively, this suggests that increased EphA4 activity in human AD could contribute to aberrant Cdk5 hyperactivation. EphA4 activation has also been found to phosphorylate and activate the Rho-GTPase activating protein (RhoGAP),  $\alpha 2$ -chimaerin to inactivate Rac1 (Shi et al., 2007). Because lower Rac1 activity has also been reported in human AD (Huang et al., 2013) and in the Tg2576 AD mouse model (Petratos et al., 2008), AD-associated EphA4 activation may also contribute to Rac1 inactivation through aberrant  $\alpha 2$ -chimaerin activation.

In addition to AD, pathological EphA4 activation has also been implicated in ALS. EphA4 was identified as a genetic modifier in a mutant SOD1 zebrafish model of ALS, in which genetic or pharmacological EphA4 inhibition reverses SOD1-mediated motor neuron toxicity (Van Hoecke et al., 2012). EphA4 expression inversely correlates with disease onset and survival in ALS patients, in whom high EphA4 levels are associated with early disease onset (Van Hoecke

et al., 2012). Interestingly, SORLA staining is attenuated in anterior horn cells from human ALS spinal cord tissue (Mori et al., 2015). Given that SORLA can inhibit pathological EphA4 activation in AD, it is tempting to speculate that reductions in SORLA may also contribute to the onset of other disorders such as ALS, potentially through a related EphA4-inactivating mechanism.

Previous studies indicated that homozygous SORLA gene inactivation significantly elevates  $A\beta$  generation in mice (Andersen et al., 2005) but has no obvious effects on basal synaptic transmission or LTP of these animals (Rohe et al., 2008). In addition, SORLA TG or KO mice appear to have no detectable cognitive abnormalities or gross anatomical aberrations within the central nervous system (Andersen et al., 2005; Caglayan et al., 2014). Although we show that SORLA can affect ephrin-mediated EphA4 activation and growth cone collapse in vitro, SORLA overexpression or deletion appears to have little detrimental effect on murine brain development (Rohe et al., 2008). This suggests that developmental redundancies are able to compensate for SORLA fluctuations in response to physiological wiring and signaling cues. The genetic implication of SORLA in age-related neurodegeneration indicates that SORLA may have a more fundamental role in protecting the adult brain from age-dependent neurodegenerative stressors than in early developmental events.

In summary, we reveal here a new role for SORLA in attenuating  $A\beta$  toxicity, which likely depends on suppressing synaptotoxic activation of EphA4. SORLA presents a unique case as an AD-related gene because it may suppress

neurotoxicity simultaneously through suppression of amyloidogenic processing and of A $\beta$  toxicity pathways. As the SORLA-dependent mechanism we describe represents a novel way of modifying the activity of cell surface A $\beta$  receptors, it will be interesting in future studies to investigate whether other cell surface A $\beta$  receptors such as the cellular prion protein, NMDAR, LirilB2, EphB2 (Laurén et al., 2009; Cissé et al., 2011; Rönicke et al., 2011; Kim et al., 2013), and others can be modulated by AD-linked transmembrane components such as SORLA.

## MATERIALS AND METHODS

### Cell culture and transfection

HEK293T and HEK293 cells stably expressing the Swedish APP KM670/671NL variant (HEKswAPP) and HEK293 cells stably expressing EphA4 (HEK-A4; provided by E. Pasquale, SBP, La Jolla, CA) were cultured in DMEM supplemented with 10% FBS. Turbofect transfection reagent (Life Technologies) was used for transient transfection of all cell lines described according to specifications from the manufacturer. RNAi MAX (Life Technologies) was used for transfection of siRNA oligonucleotides. siRNA targeting sequences to cognate human targets for cell line transfection were 5'-CTGGGATTTATCGGAGCAATA-3' for SORLA, transfected at a final concentration of 10 nM, and purchased from Qiagen. An AllStars siRNA oligo was transfected as a negative control (Qiagen).

### Primary neuronal culture

Pregnant female mice were collected from timed matings, and embryos were harvested from SORLA-Rosa26/WT BALB/c matings or SORLA KO animals at embryonic day 17 (E17)–E18. Primary cortical and hippocampal neurons were obtained by microdissection of the cerebral cortex from embryos using a stereomicroscope and dispersed by digestion in trypsin and DNaseI for 30 min at 37°C followed by trituration in DMEM. Embryonic tissue was also collected at harvesting and processed for genotype analysis for SORLA-Rosa26 neurons using the MyTaq DNA extraction and PCR genotyping system (Bioline), where WT and SORLA-Rosa26 neurons from individual embryos were maintained separately. Neurons were plated and maintained on poly-L-lysine-coated coverslips or culture dishes in Neurobasal medium supplemented with B27, glutamine, and penicillin/streptomycin. Medium was changed every 3 d (half of the medium was replaced).

### Antibodies, plasmid constructs, and purified proteins

pcDNA3 SORLA was obtained as a gift from Dr. James Lah (Emory University, Atlanta, GA). pcDNA3 SORLA-GST was generated by removal of the terminal stop codon in pcDNA3 SORLA and generating an XbaI site downstream of the SORLA ORF by site-directed mutagenesis. GST was then cloned in-frame downstream of SORLA using XbaI sites. pcDNA3 IRES-GFP was constructed by PCR amplification of an

IRES-GFP fusion fragment, which was cloned using XhoI and XbaI sites at the 3' end of pcDNA3 SORLA. SORLA Fc-fusion constructs for pull-down interaction analysis were expressed from pcDNA3, where Fc constructs were cloned in-frame with an N-terminal CD5 signal peptide sequence and a C-terminal Fc sequence (Menzel et al., 2001). SORLA cDNA fragments comprised the SORLA VPS10 (aa 1–757), YWTD repeat/EGF-like region (aa 758–1,076), LDLR class a repeats (aa 1,077–1,554), and fibronectin type III repeats (aa 1,555–2,135). The T947M SORLA mutation within the YWTD repeat/EGF-like region was introduced into full-length SORLA and pcDNA3 YWTD/EGF-like Fc constructs by site-directed mutagenesis using 5'-CATAGAGCGGATCAT GTTCAGTGGCCAGCAG-3' forward and 5'-CTGCTG GCCACTGAACATGATCCGCTCTATG-3' reverse primers.

pcDNA3 EphA4 used in this study consists of the human EphA4 cDNA cloned through 5' XhoI and 3' XbaI sites. K563R kinase dead EphA4 was generated by site-directed mutagenesis using 5'-TGTGTGGCTATCAGGACT CTGAAAGCTG-3' forward and 5'-CAGCTTTCAGAG TCCTGATAGCCACACA-3' reverse primers. pcDNA3 EphA4-FLAGhis6 was constructed by reamplifying the EphA4 ORF, with removal of the stop codon at the 3' end, and cloning a FLAGhis6 oligo 3' in-frame downstream of the EphA4 coding sequence.

Antibodies were all purchased from commercial sources: SORLA (LR11; BD Biosciences), EphA4 (S-20), EphB2 and GST polyclonal (Santa Cruz), FLAG M2 (Stratagene/Sigma),  $\beta$ -actin,  $\beta$ III-tubulin (Tuj1) and  $\alpha$ -tubulin (Sigma), EphA4 monoclonal (Life Technologies/Thermo Fisher Scientific), p-Y602 EphA4 (ECM Biosciences), EphB1 (5F10 mouse monoclonal) and pTyr100 (Cell Signaling Technology). Goat EphA4 and EphB2 (R&D Systems) were also used for immunoprecipitation experiments. PSD95 (Millipore), and MOAB-2 (Biosensis) antibodies were used for immunohistological staining. The B436 monoclonal antibody targeting the A $\beta$  region was used to detect A $\beta$  oligomers by immunoblot (Huang et al., 2016). An affinity-purified EphA4 polyclonal antibody was generated against the last 11 C-terminal residues (Lamberto et al., 2014), and the 22C11 monoclonal antibody for APP detection was purified in-house.

### Recombinant EphA4-FLAGhis6 purification and A $\beta$ oligomer preparation

EphA4-FLAGhis6 was purified from HEK293T cells transfected with pcDNA3 EphA4-FLAGhis6. Cell lysates were generated in lysis buffer containing protease inhibitors and clarified by centrifugation at 10,000 rpm for 10 min. Imidazole was added to a final concentration of 10 mM, and lysates were precipitated with Ni-NTA agarose (Qiagen) overnight, washed in 10 mM Tris-HCl, pH 8.0/0.5 M NaCl with 20 mM imidazole, and eluted in 10 mM Tris-HCl, pH 8.0/0.5 M NaCl with 0.3 M imidazole. Eluates were dialyzed in 1 $\times$  PBS and frozen for binding experiments as described in *In vitro* and *in vivo* GST and Fc pull-down assays.

Human synthetic A $\beta_{1-42}$  (Anaspec) was suspended in hexafluoroisopropanol at a concentration of 1 mM and incubated at room temperature for 1 h. The suspension was aliquoted and evaporated using a SpeedVac system for 3 h and stored at  $-80^{\circ}\text{C}$ . A $\beta$  oligomers were prepared by resuspending the A $\beta$  in dry DMSO at a concentration of 5 mM, vortexed for 30 s, and diluted in PBS 10-fold. A $\beta$  peptides were oligomerized by 10-fold dilution in PBS and incubated at  $4^{\circ}\text{C}$  for 16 h. The solution was sonicated at  $4^{\circ}\text{C}$  for 10 min in a bath sonicator, and A $\beta$  peptide solutions were centrifuged at 1,000 rpm for 2 min, with supernatants transferred to fresh tubes. Oligomerization of A $\beta_{1-42}$  was confirmed by immunoblotting.

#### In vitro and in vivo GST and Fc pull-down assays

For reconstitution of SORLA/EphA4 complexes in HEK293T cells, GST alone or GST-SORLA was expressed using pRK5mGST or pCDNA3 SORLA-GST vectors transfected in HEK293T and HEKswAPP cells. Cell lysates were generated in lysis buffer (20 mM Tris-HCl, pH 7.5, 150 mM NaCl, 10 mM MgCl<sub>2</sub>, 5% glycerol, and 1% NP-40) in the presence of protease inhibitors (Complete EDTA-free; Roche), and GST proteins were precipitated with glutathione Sepharose. Immunoblots of precipitates detected the presence of EphA4, APP, or GST components.

Mouse EphA4-Fc or Fc alone (R&D Systems) was immobilized on protein G Sepharose, washed with lysis buffer, and incubated with HEK293T lysates overexpressing SORLA. Precipitates were washed with lysis buffer and eluted with 0.2 M glycine (pH 2.5) for 20 min; eluates were analyzed by immunoblotting. For analysis of SORLA ectodomain fragment interactions with EphA4-FLAGhis6, the Fc-fusion constructs described above (Antibodies, plasmid constructs, and purified proteins) were transfected into HEK293T cells, and conditioned medium (FBS-free DMEM) was collected after secretion for 48 h. Fc proteins were purified with protein G Sepharose, with EphA4-FLAGhis6 added to immobilized Fc proteins. Precipitates were washed and immunoblotted for EphA4 or Fc.

#### Mouse lines

SORLA-Rosa26 (SORLA TG) mouse lines overexpressing SORLA through a CMV/ $\beta$ -actin promoter element was previously established (Caglayan et al., 2014). SORLA deletion (SORLA KO) mouse lines were also established previously (Andersen et al., 2005; Rohe et al., 2008) and maintained as a homozygous line for generation of primary neurons. Tg2576 mice harboring Swedish familial mutations in the human APP gene were used in preliminary immunoprecipitation experiments (Hsiao et al., 1996). All procedures involving animals were performed under the guidelines of Sanford-Burnham Medical Research Institute Institutional Animal Care and Use Committee.

#### Human brain tissue

Human brain tissue was obtained from the University of California, San Diego (courtesy of E. Masliah), and the Univer-

sity of Miami (Neurobiobank) in contract with the National Institutes of Health. Human brain samples were processed and analyzed with institutional permission in accordance with California and National Institutes of Health guidelines. Information pertaining to the human brain specimens used in this study is included in Table S1.

#### Coimmunoprecipitation assays

SORLA complexes were immunoprecipitated from mouse brain lysates in lysis buffer using 0.5  $\mu\text{g}$  antibodies as indicated, where immunocomplexes were precipitated with protein G Sepharose and washed in lysis buffer. Immunocomplexes were immunoblotted for various components as indicated.

#### Mouse and human brain biochemical fractionation and EphA4 IP analysis from synaptosomes

Mouse hippocampal tissue was processed for biochemical synaptic/PSD-enrichment analysis as described previously (Wang et al., 2013). In brief, hippocampal tissue was homogenized using a Dounce homogenizer in fractionation buffer (0.32 M sucrose, 25 mM Hepes, pH 7.4, in protease and phosphatase inhibitors), and nuclei and debris were cleared by centrifugation (500 g, 10 min). Membranes/crude synaptosomes were separated by centrifugation at 10,000 g for 12 min, and membranes were washed twice in 25 mM Hepes, pH 7.4/150 mM NaCl and solubilized in 25 mM Hepes, pH 7.4/150 mM NaCl buffer with 1% Triton X-100 and phosphatase/protease inhibitors. PSD-enriched fractions were precipitated by centrifugation at 10,000 g for 20 min, washed in 25 mM Hepes, pH 7.4/150 mM NaCl, and solubilized in 25 mM HEPES, pH 7.4/150 mM NaCl/1% Triton X-100. Human tissue from frontal cortex was similarly homogenized as described for mouse hippocampal tissue and resuspended in fractionation buffer at 0.5 ml/0.1 mg of frozen tissue.

EphA4 was immunoprecipitated in Triton X-100 solubilized synaptosomes from mouse hippocampus and human brain tissue and incubated with a mouse monoclonal antibody for EphA4 (Thermo Fisher Scientific). Protein G immunocomplexes were precipitated, washed in lysis buffer, and analyzed by immunoblot analysis.

#### EphA4 activation, growth cone collapse, and EphA4 clustering

Recombinant ephrinA1-Fc or control Fc (R&D Systems) was used to stimulate stably transfected EphA4 HEK293 (HEK-A4) cells or primary mouse neurons at a concentration of 1  $\mu\text{g}/\text{ml}$  for the times indicated to assay EphA4 kinase activation. After stimulation, cells or neurons were washed in  $1\times$  PBS and lysed in Buffer1 (20 mM Tris-HCl, pH 7.5, 150 mM NaCl, 10 mM MgCl<sub>2</sub>, 5% glycerol, and 1% NP-40) in the presence of protease inhibitors (Complete EDTA-free; Roche) and phosphatase inhibitors (Pierce). EphA4 was then immunoprecipitated for 3–5 h at  $4^{\circ}\text{C}$  using EphA4 antibodies (Life Technologies) and protein G Sepharose; beads were washed four times with Buffer1 and immuno-

blotted for EphA4 or phosphorylation of the p-Y602 residue to determine activation.

Growth cone collapse in cultured hippocampal neurons was assayed as described previously (Richter et al., 2007). In brief, ephrinA1-Fc or human Fc control was preclustered with anti-human Fc (1:10), and hippocampal neurons on glass coverslips grown at low density were exposed to 1  $\mu$ g/ml ephrinA1-Fc or control Fc for 0.5 h at 3 d in vitro (DIV3). Neurons were then fixed in 4% PFA, permeabilized in 0.5% Triton X-100/1 $\times$  PBS, and blocked in 3% BSA. Neuronal growth cones were stained with  $\beta$ III-tubulin (Tuj1) antibodies and an Alexa Fluor 488-conjugated goat anti-rabbit antibody/Alexa Fluor 568 phalloidin. Growth cones were tracked along the longest axonal process, and growth cone images were obtained for all neurons imaged on a single coverslip. Growth cones were classified into collapsed and non-collapsed categories according to the presence or absence of F-actin-rich lamellipodial and filopodial extensions within the growth cone area. A total of 252 (WT), 168 (SORLA TG), and 153 (SORLA KO) growth cones were scored over multiple embryos from a minimum of three experiments derived from two separate embryonic neuronal cultures for growth cone collapse.

EphA4 clustering was visualized in cultured hippocampal neurons as described previously (Shi et al., 2007), with modification. Preclustered EphrinA1-Fc or Fc control was incubated with DIV3 hippocampal neurons grown on coverslips for 5 or 30 min. Neurons were fixed in 4% PFA and stained with EphA4 (S-20, Santa Cruz)/ $\alpha$ -tubulin (Sigma) antibodies, followed by fluorescent secondary antibodies and Alexa Fluor 350 phalloidin. EphrinA1-Fc treatment for 5 min did not induce growth cone collapse but did initiate EphA4 clustering in WT neurons. Growth cone regions were tracked along axonal extensions, and EphA4 staining was homogeneously normalized for intensity in all neurons for each experiment using identical image acquisition settings; EphA4 clusters at least 0.2  $\mu$ m in size were scored within each F-actin-rich growth cone area per neuron. A minimum of three experiments were scored from two independent embryonic neuronal dissections; a total of 33 WT, 29 SORLA TG, and 38 SORLA KO growth cone regions were quantified.

### Cell surface biotinylation

Cell surface biotinylation using EZ-link Sulfo-NHS-LC biotin in HEK293T and primary neurons was performed as described previously (Wang et al., 2013). In HEK293T, cells were first either cotransfected with vectors overexpressing SORLA and EphA4 or sequentially transfected with control/SORLA siRNA oligos and subsequently transfected with an EphA4 overexpression vector. For surface biotin labeling, cells or neurons were washed in cold 1 $\times$  PBS supplemented with 1 mM MgCl<sub>2</sub>/1.3 mM CaCl<sub>2</sub> (1 $\times$  PBS/CM) and incubated with 500  $\mu$ g/ml biotin labeling reagent in 1 $\times$  PBS/CM at 4°C with agitation. Labeling was repeated and quenched with 7.5  $\mu$ g/ml glycine in 1 $\times$  PBS/CM. Cells were washed, lysed in

lysis buffer, and incubated overnight with streptavidin agarose at 4°C with agitation. Streptavidin agarose beads were then washed and boiled in Laemmli buffer, and biotin-labeled precipitates were visualized and quantified by immunoblotting.

### Stereotactic hippocampal A $\beta$ injection

A $\beta$ <sub>1-42</sub> oligomers (2  $\mu$ l, 500  $\mu$ M) or PBS vehicle controls were stereotactically injected at a rate of 0.5  $\mu$ l/min into the hippocampus of anesthetized SORLA TG mice or WT littermate animals using the following coordinates: anterior posterior, -2.0 mm; medial lateral,  $\pm$ 1.3 mm; dorsal ventral, 2.1 mm. Mice were allowed to recover for 1 wk after injection and then were subjected to behavioral analysis (see Mouse behavioral analysis). Animals were immediately killed after behavioral analysis, and dissected hippocampus tissue was processed for biochemical analysis. For immunohistological analysis, mice were killed 4 d after injection and processed as specified in Immunohistochemistry and detection of EphA4/PSD95 puncta in mouse sections.

### Mouse behavioral analysis

A modified Morris water maze apparatus (San Diego Instruments) was used to evaluate spatial reference learning and memory (Billings et al., 2005; Vorhees and Williams, 2006). For 5 d, mice were trained to escape to an invisible 14-cm-diameter platform submerged 1.5 cm beneath the water surface, which was obscured using nontoxic white paint; in case of failure to find the platform within 60 s, animals were guided to the platform and allowed to remain there for 10 s. The escape latency was scored as 60 s in instances in which the mice were unable to find the platform. Because of the large cohort size tested, mice were given two trials per day, and retention of spatial training (probe test) was assessed 24 h after the final training trial. Each mouse was assayed using a single probe test comprising a 60-s free swim session in the pool where the platform was removed. The time spent in each quadrant was recorded, as well as the number of times the mice entered the platform area. The ANY-maze video tracking system (Stoelting Co.) was used for automated trial acquisition and analysis of all trials. A total of 48 mice ( $n = 12$  each for WT and SORLA TG genotypes injected with either PBS or A $\beta$ ) were subjected to Morris water maze analysis.

### A $\beta$ <sub>1-42</sub> ELISA

Hippocampal tissue from human A $\beta$ <sub>1-42</sub>-injected WT and SORLA TG animals subjected to Morris water maze analysis were subsequently processed for biochemical EphA4 activation as described in Mouse and human brain biochemical fractionation and EphA4 IP analysis from synaptosomes, where A $\beta$  was extracted from total hippocampal protein preparations in RIPA buffer (10 mM Tris-HCl, pH 8, 1 mM EDTA, 1% Triton X-100, 0.1% Na deoxycholate, 0.1% SDS, 140 mM NaCl, and 1 mM PMSF), and human A $\beta$ <sub>1-42</sub> levels were measured using a commercial human A $\beta$ <sub>1-42</sub> ELISA system (Invitrogen). Normalized protein levels used for ELISA

analysis were quantified for A $\beta$ <sub>1–42</sub> concentrations, and relative A $\beta$ <sub>1–42</sub> values were calculated with WT A $\beta$ <sub>1–42</sub> set to 1.0.

### Immunohistochemistry and detection of EphA4/PSD95 puncta in mouse sections

For immunohistological detection of A $\beta$ , WT and SORLA TG mice were anesthetized and subjected to intracardial perfusion with PBS and fixation with 4% PFA. The tissues were cryoprotected in 30% sucrose, embedded in O.C.T. (Tissue Tek), and subjected to cryostat sectioning. Free-floating tissue sections (20  $\mu$ m) were immunostained using the MOAB A $\beta$  antibody and subsequently incubated with an anti-mouse HRP secondary antibody, and developed using a DAB substrate (Vector Laboratories). Sections were counterstained with hematoxylin, and images were acquired using a ScanScope AT2 system.

Mouse sections were scored for colocalizing overlap of EphA4 and PSD95 foci in 100- $\mu$ m-square areas within the dentate gyrus region by scoring the number of overlapping foci over the total EphA4 and PSD95 foci in five regions for PBS and A $\beta$  injections in WT and SORLA TG animals.

### Electrophysiology

For analysis of LTP, ex vivo hippocampal slices were prepared from 3-mo-old WT and SORLA TG mice in the presence or absence of 500 nM oligomerized A $\beta$ , similar to methods described previously (Fu et al., 2014). Mice were decapitated under deep terminal anesthesia, and brains were surgically removed in ice-cold, sucrose-based artificial cerebrospinal fluid (aCSF) of the following composition: 190 mM sucrose, 25 mM D-glucose; 25 mM NaHCO<sub>3</sub>, 3 mM KCl, 1.25 mM NaH<sub>2</sub>PO<sub>4</sub>, 5 mM MgSO<sub>4</sub>, 10 mM NaCl, and 0.5 mM CaCl<sub>2</sub> saturated with carbogen (95% O<sub>2</sub>/5% CO<sub>2</sub>) to pH 7.4. A vibrating-blade microtome (Leica VT1000S) was used to cut 400- $\mu$ m-thick coronal slices containing both cortex and hippocampus. Slices were transferred to a holding chamber containing warm (34°C) aCSF of the following composition: 125 mM NaCl, 25 mM NaHCO<sub>3</sub>, 3.0 mM KCl, 1.25 mM NaH<sub>2</sub>PO<sub>4</sub>, 2.0 mM CaCl<sub>2</sub>, 1.0 mM MgSO<sub>4</sub>, and 10 mM D-glucose saturated with carbogen (95% O<sub>2</sub>/5% CO<sub>2</sub>) to pH 7.4. Slices were left to recover at room temperature in oxygenated aCSF in the presence or absence of 500 nM oligomerized A $\beta$  for at least 2 h before induction of LTP. For recording, slices were transferred to a recording chamber and perfused with warm (32°C) oxygenated aCSF at a rate of 2 ml/min. For recording, both stimulating and recording electrodes were positioned within hippocampal CA1 subfield (stratum radiatum) on an upright microscope (BX51WI; Olympus). An electrical stimulation protocol was used to evoke field excitatory postsynaptic potentials (fEPSPs) in CA1 pyramidal neurons by activating Schäffer collateral axonal fibers located in the stratum radiatum. LTP was induced by two trains of high-frequency stimulation (100 Hz for 1 s at 30-s intervals) using a concentric bipolar stimulating electrode (CBARC75; FHC). fEPSPs were recorded

using glass electrodes filled with aCSF and placed in the CA1 stratum radiatum (dendritic region). All recordings of synaptic activity were performed using a Multiclamp 700B (Molecular Devices), and signals were filtered at 3 kHz, digitized, and sampled using pClamp10 software (Molecular Devices). The magnitude of potentiation was calculated as percentage change in fEPSP slope normalized to baseline values. The mean change in synaptic potentiation 1 h after induction of LTP was used to compare different experimental groups. For each genotype/treatment, five slices from three mice were processed for electrophysiological analysis.

### Cell and neuronal image sample preparation and acquisition

Hippocampal neuronal images for growth cone collapse and neuronal/cellular EphA4 clustering were acquired using an inverted Zeiss Axio Observer Z1 fluorescence microscopy system using a CCD sensicam (PCO; Kelheim), where acquisition and processing of images used Slidebook 5.5 software. All images were acquired using a 40 $\times$  air objective lens (0.75 NA), and images were exported as 8-bit tiffs for further analysis using ImageJ. Cultured HEK293T transfected with vectors expressing EphA4-GFP were seeded and manipulated (untreated or treated with 500 nM A $\beta$  oligomers for 2 h) on poly-L-lysine coated glass coverslips and fixed in 4% PFA. After permeabilization in 0.5% Triton X-100 in 1 $\times$  PBS, coverslips were washed, blocked in 3% BSA, and stained in primary and fluorescent secondary antibodies before mounting in Prolong Gold antifade on glass slides.

For live cell imaging of EphA4, vectors expressing EphA4-mCherry and GFP alone or SORLA-IRES-GFP were transfected into HEK293T cells in glass-bottom tissue culture dishes coated with poly-L-lysine 24 h after transfection. Cells were imaged before the addition of A $\beta$  oligomers and subsequently imaged using a Zeiss 710 confocal microscope 63 $\times$  oil lens. Images were captured at 1 frame/min for 35 min.

### Statistical analyses

All statistical analyses used in this study determined the significant differences between two groups using nonpaired *t* tests with equal variance from a minimum of three experiments unless stated differently. Statistical significance was calculated using GraphPad Prism 7.0 for all animal and human tissue and behavioral analyses.

### Online supplemental material

Fig. S1 shows immunoprecipitation of SORLA with an EphA4 antibody, interaction of the EphA4 ectodomain with SORLA, phosphorylation of EphA4 and SORLA in HEK293T cells, and measurement of ephrinA1-induced EphA4 phosphorylation kinetics. Fig. S2 shows comparative cell surface EphA4 levels with SORLA modulation and EphA4 levels in total and postsynaptic brain fractions. Fig. S3 depicts purified EphA4 and EphA4 distribution in HEK293T cells with A $\beta$  treatment and human A $\beta$  levels after stereotactic hippocampal injection in WT and SORLA TG mice. Fig.

S4 presents a model for SORLA-dependent EphA4 inhibition in response to ephrinA1 and A $\beta$ , analysis of total SORLA levels, and EphA4/SORLA interaction in human control and AD brain samples. Table S1 lists all the human brain tissues used in this study.

## ACKNOWLEDGMENTS

We thank Viridiana Ylis for animal support and the Xu laboratory at Sanford Burnham Prebys Medical Discovery Institute for technical assistance and helpful discussion. Special thanks to Ivy Trinh (UCSD) for assistance with human brain tissue and to Drs. Ilaria Lamberto and Elena Rubio de la Torre for providing the EphA4 HEK293 stable cell line.

This work was supported in part by grants from National Institutes of Health (R01AG021173, R01AG038710, R01AG044420, and R01NS046673 to H. Xu; R01AG18440, R01AG5131, R01AG11385, and R01NS076411 to E. Masliah; R01NS087070 to E.B. Pasquale), the Alzheimer's Association (H. Xu), The Tanz Family Funds (H. Xu and E.B. Pasquale), the Cure Alzheimer's Fund (H. Xu), and a Shiley-Marcos Alzheimer's Disease Research Center, University of California, San Diego Grant (ADRC 2015 59226 to T.Y. Huang).

The authors declare no competing financial interests.

Author contributions: T.Y. Huang and H. Xu conceived the study. T.Y. Huang designed, performed, and analyzed the majority of the experiments described. T.Y. Huang and X. Li performed stereotactic injection procedures and behavioral tests. T.Y. Huang processed mouse and human brain tissue for biochemical analysis. Y. Zhao and L.-I. Jiang processed mouse brain samples for immunohistology and biochemical analysis and performed confocal microscopy procedures. Y. Liu, Y. Sun, and J.C. Piña-Crespo performed the electrophysiology analysis. B. Zhu performed live cell imaging experiments. E.B. Pasquale, E. Masliah, and T.E. Willnow provided materials essential to this study and provided advice in experimental procedures. Y. Zhao provided important discussion. T.Y. Huang and H. Xu wrote the manuscript, and all authors approved the submitted manuscript.

Submitted: 7 August 2017

Revised: 12 September 2017

Accepted: 15 September 2017

## REFERENCES

Andersen, O.M., J. Reiche, V. Schmidt, M. Gotthardt, R. Spoelgen, J. Behlke, C.A. von Arnim, T. Breiderhoff, P. Jansen, X. Wu, et al. 2005. Neuronal sorting protein-related receptor sorLA/LR11 regulates processing of the amyloid precursor protein. *Proc. Natl. Acad. Sci. USA.* 102:13461–13466. <https://doi.org/10.1073/pnas.0503689102>

Audrain, M., R. Fol, P. Dutar, B. Potier, J.M. Billard, J. Flament, S. Alves, M.A. Burlot, G. Dufayet-Chaffaud, A.P. Bemelmans, et al. 2016. Alzheimer's disease-like APP processing in wild-type mice identifies synaptic defects as initial steps of disease progression. *Mol. Neurodegener.* 11:5. <https://doi.org/10.1186/s13024-016-0070-y>

Billings, L.M., S. Oddo, K.N. Green, J.L. McLaugh, and F.M. LaFerla. 2005. Intraneuronal A $\beta$  causes the onset of early Alzheimer's disease-related cognitive deficits in transgenic mice. *Neuron.* 45:675–688. <https://doi.org/10.1016/j.neuron.2005.01.040>

Caglayan, S., S. Takagi-Niidome, F. Liao, A.S. Carlo, V. Schmidt, T. Burgert, Y. Kitago, E.M. Fuchtbauer, A. Fuchtbauer, D.M. Holtzman, et al. 2014. Lysosomal sorting of amyloid- $\beta$  by the SORLA receptor is impaired by a familial Alzheimer's disease mutation. *Sci. Transl. Med.* 6:223ra20. <https://doi.org/10.1126/scitranslmed.3007747>

Carmona, M.A., K.K. Murai, L. Wang, A.J. Roberts, and E.B. Pasquale. 2009. Glial ephrin-A3 regulates hippocampal dendritic spine morphology and glutamate transport. *Proc. Natl. Acad. Sci. USA.* 106:12524–12529. <https://doi.org/10.1073/pnas.0903328106>

Cissé, M., B. Halabisky, J. Harris, N. Devidze, D.B. Dubal, B. Sun, A. Orr, G. Lotz, D.H. Kim, P. Hamto, et al. 2011. Reversing EphB2 depletion rescues cognitive functions in Alzheimer model. *Nature.* 469:47–52. <https://doi.org/10.1038/nature09635>

Egea, J., U.V. Nissen, A. Dufour, M. Sahin, P. Greer, K. Kullander, T.D. Mrcic-Flogel, M.E. Greenberg, O. Kiehn, P. Vanderhaeghen, and R. Klein. 2005. Regulation of EphA 4 kinase activity is required for a subset of axon guidance decisions suggesting a key role for receptor clustering in Eph function. *Neuron.* 47:515–528. <https://doi.org/10.1016/j.neuron.2005.06.029>

Filosa, A., S. Paixão, S.D. Honsek, M.A. Carmona, L. Becker, B. Feddersen, L. Gaitanos, Y. Rudhard, R. Schoepfer, T. Klopstock, et al. 2009. Neuron-glia communication via EphA4/ephrin-A3 modulates LTP through glial glutamate transport. *Nat. Neurosci.* 12:1285–1292. <https://doi.org/10.1038/nn.2394>

Fjorback, A.W., M. Seaman, C. Gustafsen, A. Mehmedbasic, S. Gokool, C. Wu, D. Militz, V. Schmidt, P. Madsen, J.R. Nyengaard, et al. 2012. Retromer binds the FANSHY sorting motif in SorLA to regulate amyloid precursor protein sorting and processing. *J. Neurosci.* 32:1467–1480. <https://doi.org/10.1523/JNEUROSCI.2272-11.2012>

Fu, A.K., K.W. Hung, H. Huang, S. Gu, Y. Shen, E.Y. Cheng, F.C. Ip, X. Huang, W.Y. Fu, and N.Y. Ip. 2014. Blockade of EphA4 signaling ameliorates hippocampal synaptic dysfunctions in mouse models of Alzheimer's disease. *Proc. Natl. Acad. Sci. USA.* 111:9959–9964. <https://doi.org/10.1073/pnas.1405803111>

Fu, W.Y., Y. Chen, M. Sahin, X.S. Zhao, L. Shi, J.B. Bikoff, K.O. Lai, W.H. Yung, A.K. Fu, M.E. Greenberg, and N.Y. Ip. 2007. Cdk5 regulates EphA4-mediated dendritic spine retraction through an ephexin1-dependent mechanism. *Nat. Neurosci.* 10:67–76. <https://doi.org/10.1038/nn1811>

Glerup, S., M. Lume, D. Olsen, J.R. Nyengaard, C.B. Vaegter, C. Gustafsen, E.I. Christensen, M. Kjolby, A. Hay-Schmidt, D. Bender, et al. 2013. SorLA controls neurotrophic activity by sorting of GDNF and its receptors GFR $\alpha$ 1 and RET. *Cell Reports.* 3:186–199. <https://doi.org/10.1016/j.celrep.2012.12.011>

Hruska, M., and M.B. Dalva. 2012. Ephrin regulation of synapse formation, function and plasticity. *Mol. Cell. Neurosci.* 50:35–44. <https://doi.org/10.1016/j.mcn.2012.03.004>

Hsiao, K., P. Chapman, S. Nilsen, C. Eckman, Y. Harigaya, S. Younkin, F. Yang, and G. Cole. 1996. Correlative memory deficits, A $\beta$  elevation, and amyloid plaques in transgenic mice. *Science.* 274:99–102. <https://doi.org/10.1126/science.274.5284.99>

Huang, T.Y., S. Michael, T. Xu, A. Sarkeshik, J.J. Moresco, J.R. Yates III, E. Masliah, G.M. Bokoch, and C. DerMardirossian. 2013. A novel Rac1 GAP splice variant relays poly-Ub accumulation signals to mediate Rac1 inactivation. *Mol. Biol. Cell.* 24:194–209. <https://doi.org/10.1091/mbc.E12-07-0565>

Huang, T.Y., Y. Zhao, X. Li, X. Wang, I.C. Tseng, R. Thompson, S. Tu, T.E. Willnow, Y.W. Zhang, and H. Xu. 2016. SNX27 and SORLA interact to reduce amyloidogenic subcellular distribution and processing of amyloid precursor protein. *J. Neurosci.* 36:7996–8011. <https://doi.org/10.1523/JNEUROSCI.0206-16.2016>

Kim, T., G.S. Vidal, M. Djuricic, C.M. William, M.E. Birnbaum, K.C. Garcia, B.T. Hyman, and C.J. Shatz. 2013. Human LirB2 is a  $\beta$ -amyloid receptor and its murine homolog PirB regulates synaptic plasticity in an Alzheimer's model. *Science.* 341:1399–1404. <https://doi.org/10.1126/science.1242077>

Kitago, Y., M. Nagae, Z. Nakata, M. Yagi-Utsumi, S. Takagi-Niidome, E. Mihara, T. Nogi, K. Kato, and J. Takagi. 2015. Structural basis for amyloidogenic peptide recognition by sorLA. *Nat. Struct. Mol. Biol.* 22:199–206. <https://doi.org/10.1038/nsmb.2954>

Lamberto, I., B.C. Lechtenberg, E.J. Olson, P.D. Mace, P.E. Dawson, S.J. Riedel, and E.B. Pasquale. 2014. Development and structural analysis of a

- nanomolar cyclic peptide antagonist for the EphA4 receptor. *ACS Chem. Biol.* 9:2787–2795. <https://doi.org/10.1021/cb500677x>
- Larsen, J.V., A.M. Kristensen, L.T. Pallesen, J. Bauer, C.B. Vægter, M.S. Nielsen, P. Madsen, and C.M. Petersen. 2016. Cytokine-like factor 1, an essential facilitator of cardiotrophin-like cytokine: ciliary neurotrophic factor receptor  $\alpha$  signaling and sorLA-mediated turnover. *Mol. Cell. Biol.* 36:1272–1286. <https://doi.org/10.1128/MCB.00917-15>
- Laurén, J., D.A. Gimbel, H.B. Nygaard, J.W. Gilbert, and S.M. Strittmatter. 2009. Cellular prion protein mediates impairment of synaptic plasticity by amyloid-beta oligomers. *Nature*. 457:1128–1132. <https://doi.org/10.1038/nature07761>
- Lee, K.Y., A.W. Clark, J.L. Rosales, K. Chapman, T. Fung, and R.N. Johnston. 1999. Elevated neuronal Cdc2-like kinase activity in the Alzheimer disease brain. *Neurosci. Res.* 34:21–29. [https://doi.org/10.1016/S0168-0102\(99\)00026-7](https://doi.org/10.1016/S0168-0102(99)00026-7)
- Louwensheimer, E., P.E. Cohn-Hokke, Y.A. Pijnenburg, M.M. Weiss, E.A. Sistermans, A.J. Rozemuller, M. Hulsman, J.C. van Swieten, C.M. van Duijn, F. Barkhof, et al. 2017. Rare genetic variant in SORL1 may increase penetrance of Alzheimer's disease in a family with several generations of APOE- $\epsilon$ 4 homozygosity. *J. Alzheimers Dis.* 56:63–74. <https://doi.org/10.3233/JAD-160091>
- Lukiw, W.J. 2012. Amyloid beta (A $\beta$ ) peptide modulators and other current treatment strategies for Alzheimer's disease (AD). *Expert Opin. Emerg. Drugs*. 17:43–60. <https://doi.org/10.1517/14728214.2012.672559>
- Marttinen, M., K.M. Kurkinen, H. Soinen, A. Haapasalo, and M. Hiltunen. 2015. Synaptic dysfunction and septin protein family members in neurodegenerative diseases. *Mol. Neurodegener.* 10:16. <https://doi.org/10.1186/s13024-015-0013-z>
- Menzel, P., F. Valencia, P. Godement, V.C. Dodelet, and E.B. Pasquale. 2001. Ephrin-A6, a new ligand for EphA receptors in the developing visual system. *Dev. Biol.* 230:74–88. <https://doi.org/10.1006/dbio.2000.0109>
- Mori, F., Y. Miki, K. Tanji, A. Kakita, H. Takahashi, J. Utsumi, H. Sasaki, and K. Wakabayashi. 2015. Sortilin-related receptor CNS expressed 2 (SorCS2) is localized to Bunina bodies in amyotrophic lateral sclerosis. *Neurosci. Lett.* 608:6–11. <https://doi.org/10.1016/j.neulet.2015.09.030>
- Murai, K.K., L.N. Nguyen, F. Irie, Y. Yamaguchi, and E.B. Pasquale. 2003. Control of hippocampal dendritic spine morphology through ephrin-A3/EphA4 signaling. *Nat. Neurosci.* 6:153–160. <https://doi.org/10.1038/nn994>
- Nicolas, G., C. Charbonnier, D. Wallon, O. Quenez, C. Bellenguez, B. Grenier-Boley, S. Rousseau, A.C. Richard, A. Rovelet-Lecrux, K. Le Guennec, et al. CNR-MAJ collaborators. 2016. SORL1 rare variants: A major risk factor for familial early-onset Alzheimer's disease. *Mol. Psychiatry*. 21:831–836. <https://doi.org/10.1038/mp.2015.121>
- Pasquale, E.B. 2005. Eph receptor signalling casts a wide net on cell behaviour. *Nat. Rev. Mol. Cell Biol.* 6:462–475. <https://doi.org/10.1038/nrm1662>
- Pasquale, E.B. 2008. Eph-ephrin bidirectional signaling in physiology and disease. *Cell*. 133:38–52. <https://doi.org/10.1016/j.cell.2008.03.011>
- Petratos, S., Q.X. Li, A.J. George, X. Hou, M.L. Kerr, S.E. Unabia, I. Hatzinisiriou, D. Maksiel, M.I. Aguilar, and D.H. Small. 2008. The beta-amyloid protein of Alzheimer's disease increases neuronal CRMP-2 phosphorylation by a Rho-GTP mechanism. *Brain*. 131:90–108. <https://doi.org/10.1093/brain/awm260>
- Pottier, C., D. Hannequin, S. Coutant, A. Rovelet-Lecrux, D. Wallon, S. Rousseau, S. Legallic, C. Paquet, S. Bombois, J. Pariente, et al. PHRC GMAJ Collaborators. 2012. High frequency of potentially pathogenic SORL1 mutations in autosomal dominant early-onset Alzheimer disease. *Mol. Psychiatry*. 17:875–879. <https://doi.org/10.1038/mp.2012.15>
- Richter, M., K.K. Murai, C. Bourgin, D.T. Pak, and E.B. Pasquale. 2007. The EphA4 receptor regulates neuronal morphology through SPAR-mediated inactivation of Rap GTPases. *J. Neurosci.* 27:14205–14215. <https://doi.org/10.1523/JNEUROSCI.2746-07.2007>
- Rogaeva, E., Y. Meng, J.H. Lee, Y. Gu, T. Kawarai, F. Zou, T. Katayama, C.T. Baldwin, R. Cheng, H. Hasegawa, et al. 2007. The neuronal sortilin-related receptor SORL1 is genetically associated with Alzheimer disease. *Nat. Genet.* 39:168–177. <https://doi.org/10.1038/ng1943>
- Rohe, M., A.S. Carlo, H. Breyhan, A. Sporbert, D. Militz, V. Schmidt, C. Wozny, A. Harmeier, B. Erdmann, K.R. Bales, et al. 2008. Sortilin-related receptor with A-type repeats (SORLA) affects the amyloid precursor protein-dependent stimulation of ERK signaling and adult neurogenesis. *J. Biol. Chem.* 283:14826–14834. <https://doi.org/10.1074/jbc.M710574200>
- Rohe, M., D. Hartl, A.N. Fjorback, J. Klose, and T.E. Willnow. 2013. SORLA-mediated trafficking of TrkB enhances the response of neurons to BDNF. *PLoS One*. 8:e72164. <https://doi.org/10.1371/journal.pone.0072164>
- Rönicke, R., M. Mikhaylova, S. Rönicke, J. Meinhardt, U.H. Schröder, M. Fändrich, G. Reiser, M.R. Kreutz, and K.G. Reymann. 2011. Early neuronal dysfunction by amyloid  $\beta$  oligomers depends on activation of NR2B-containing NMDA receptors. *Neurobiol. Aging*. 32:2219–2228. <https://doi.org/10.1016/j.neurobiolaging.2010.01.011>
- Rosenberger, A.F., A.J. Rozemuller, W.M. van der Flier, P. Scheltens, S.M. van der Vies, and J.J. Hoozemans. 2014. Altered distribution of the EphA4 kinase in hippocampal brain tissue of patients with Alzheimer's disease correlates with pathology. *Acta Neuropathol. Commun.* 2:79. <https://doi.org/10.1186/s40478-014-0079-9>
- Scherzer, C.R., K. Offe, M. Gearing, H.D. Rees, G. Fang, C.J. Heilman, C. Schaller, H. Bujo, A.I. Levey, and J.J. Lah. 2004. Loss of apolipoprotein E receptor LR11 in Alzheimer disease. *Arch. Neurol.* 61:1200–1205. <https://doi.org/10.1001/archneur.61.8.1200>
- Schmidt, V., K. Baum, A. Lao, K. Rateitschak, Y. Schmitz, A. Teichmann, B. Wiesner, C.M. Petersen, A. Nykjaer, J. Wolf, et al. 2012. Quantitative modelling of amyloidogenic processing and its influence by SORLA in Alzheimer's disease. *EMBO J.* 31:187–200. <https://doi.org/10.1038/emboj.2011.352>
- Schmidt, V., N. Schulz, X. Yan, A. Schürmann, S. Kempa, M. Kern, M. Blüher, M.N. Poy, G. Olivecrona, and T.E. Willnow. 2016. SORLA facilitates insulin receptor signaling in adipocytes and exacerbates obesity. *J. Clin. Invest.* 126:2706–2720. <https://doi.org/10.1172/JCI84708>
- Shamah, S.M., M.Z. Lin, J.L. Goldberg, S. Estrach, M. Sahin, L. Hu, M. Bazalakova, R.L. Neve, G. Corfas, A. Debant, and M.E. Greenberg. 2001. EphA receptors regulate growth cone dynamics through the novel guanine nucleotide exchange factor ephexin. *Cell*. 105:233–244. [https://doi.org/10.1016/S0092-8674\(01\)00314-2](https://doi.org/10.1016/S0092-8674(01)00314-2)
- Shen, L., S. Kim, S.L. Risacher, K. Nho, S. Swaminathan, J.D. West, T. Foroud, N. Pankratz, J.H. Moore, C.D. Sloan, et al. Alzheimer's Disease Neuroimaging Initiative. 2010. Whole genome association study of brain-wide imaging phenotypes for identifying quantitative trait loci in MCI and AD: A study of the ADNI cohort. *Neuroimage*. 53:1051–1063. <https://doi.org/10.1016/j.neuroimage.2010.01.042>
- Shi, L., W.Y. Fu, K.W. Hung, C. Porchetta, C. Hall, A.K. Fu, and N.Y. Ip. 2007. Alpha2-chimaerin interacts with EphA4 and regulates EphA4-dependent growth cone collapse. *Proc. Natl. Acad. Sci. USA*. 104:16347–16352. <https://doi.org/10.1073/pnas.0706626104>
- Simón, A.M., R.L. de Maturana, A. Ricobaraza, L. Schiapparelli, M. Cuadrado-Tejedor, A. Pérez-Mediavilla, J. Avila, J. Del Río, and D. Frechilla. 2009. Early changes in hippocampal Eph receptors precede the onset of memory decline in mouse models of Alzheimer's disease. *J. Alzheimers Dis.* 17:773–786. <https://doi.org/10.3233/JAD-2009-1096>
- Spoelgen, R., C.A. von Arnim, A.V. Thomas, I.D. Peltan, M. Koker, A. Deng, M.C. Irizarry, O.M. Andersen, T.E. Willnow, and B.T. Hyman. 2006. Interaction of the cytosolic domains of sorLA/LR11 with the amyloid precursor protein (APP) and beta-secretase beta-site APP-cleaving enzyme. *J. Neurosci.* 26:418–428. <https://doi.org/10.1523/JNEUROSCI.3882-05.2006>

- Tseng, H.C., Y. Zhou, Y. Shen, and L.H. Tsai. 2002. A survey of Cdk5 activator p35 and p25 levels in Alzheimer's disease brains. *FEBS Lett.* 523:58–62. [https://doi.org/10.1016/S0014-5793\(02\)02934-4](https://doi.org/10.1016/S0014-5793(02)02934-4)
- Tu, S., S. Okamoto, S.A. Lipton, and H. Xu. 2014. Oligomeric A $\beta$ -induced synaptic dysfunction in Alzheimer's disease. *Mol. Neurodegener.* 9:48. <https://doi.org/10.1186/1750-1326-9-48>
- Van Hoecke, A., L. Schoonaert, R. Lemmens, M. Timmers, K.A. Staats, A.S. Laird, E. Peeters, T. Philips, A. Goris, B. Dubois, et al. 2012. EPHA4 is a disease modifier of amyotrophic lateral sclerosis in animal models and in humans. *Nat. Med.* 18:1418–1422. <https://doi.org/10.1038/nm.2901>
- Vardarajan, B.N., Y. Zhang, J.H. Lee, R. Cheng, C. Bohm, M. Ghani, C. Reitz, D. Reyes-Dumeyer, Y. Shen, E. Rogaeva, et al. 2015. Coding mutations in SORL1 and Alzheimer disease. *Ann. Neurol.* 77:215–227. <https://doi.org/10.1002/ana.24305>
- Vargas, L.M., N. Leal, L.D. Estrada, A. González, F. Serrano, K. Araya, K. Gysling, N.C. Inestrosa, E.B. Pasquale, and A.R. Alvarez. 2014. EphA4 activation of c-Abl mediates synaptic loss and LTP blockade caused by amyloid- $\beta$  oligomers. *PLoS One.* 9:e92309. <https://doi.org/10.1371/journal.pone.0092309>
- Vorhees, C.V., and M.T. Williams. 2006. Morris water maze: Procedures for assessing spatial and related forms of learning and memory. *Nat. Protoc.* 1:848–858. <https://doi.org/10.1038/nprot.2006.116>
- Wang, X., Y. Zhao, X. Zhang, H. Badie, Y. Zhou, Y. Mu, L.S. Loo, L. Cai, R.C. Thompson, B. Yang, et al. 2013. Loss of sorting nexin 27 contributes to excitatory synaptic dysfunction by modulating glutamate receptor recycling in Down's syndrome. *Nat. Med.* 19:473–480. <https://doi.org/10.1038/nm.3117>
- Yan, L., Y. Chen, W. Li, X. Huang, H. Badie, F. Jian, T. Huang, Y. Zhao, S.N. Cohen, L. Li, et al. 2016. RPS23RG1 reduces A $\beta$  oligomer-induced synaptic and cognitive deficits. *Sci. Rep.* 6:18668. <https://doi.org/10.1038/srep18668>
- Zhang, Y.W., R. Thompson, H. Zhang, and H. Xu. 2011. APP processing in Alzheimer's disease. *Mol. Brain.* 4:3. <https://doi.org/10.1186/1756-6606-4-3>

SUPPLEMENTAL MATERIAL

Huang et al., <https://doi.org/10.1084/jem.20171413>

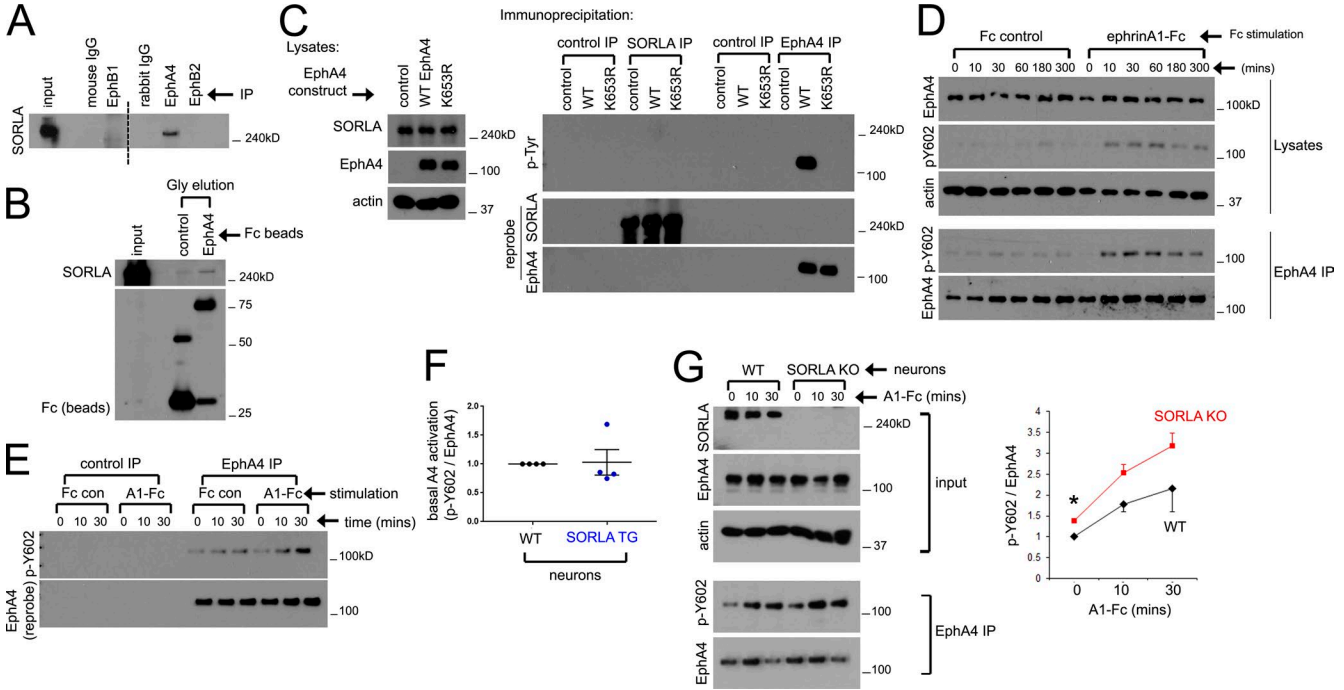
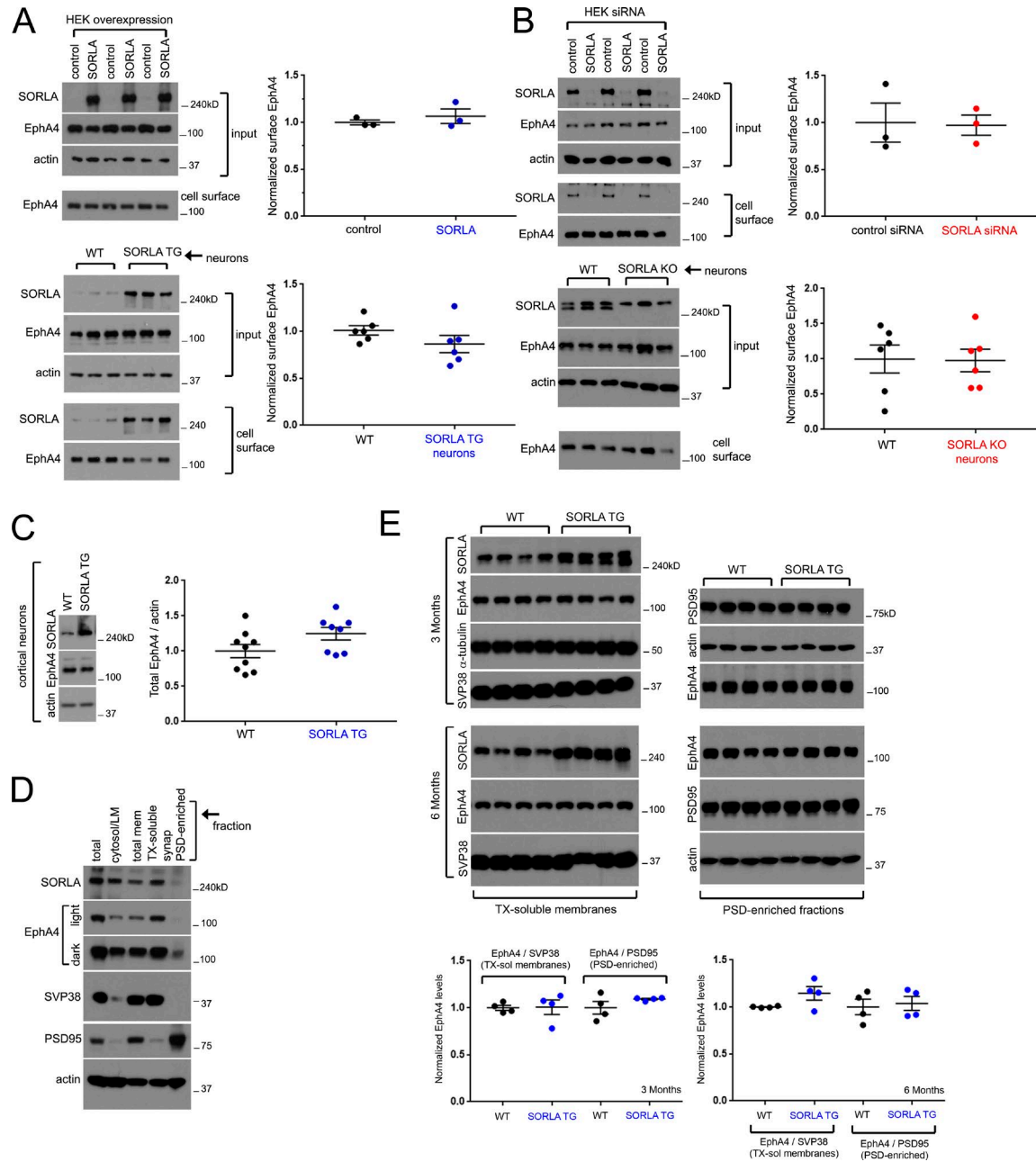
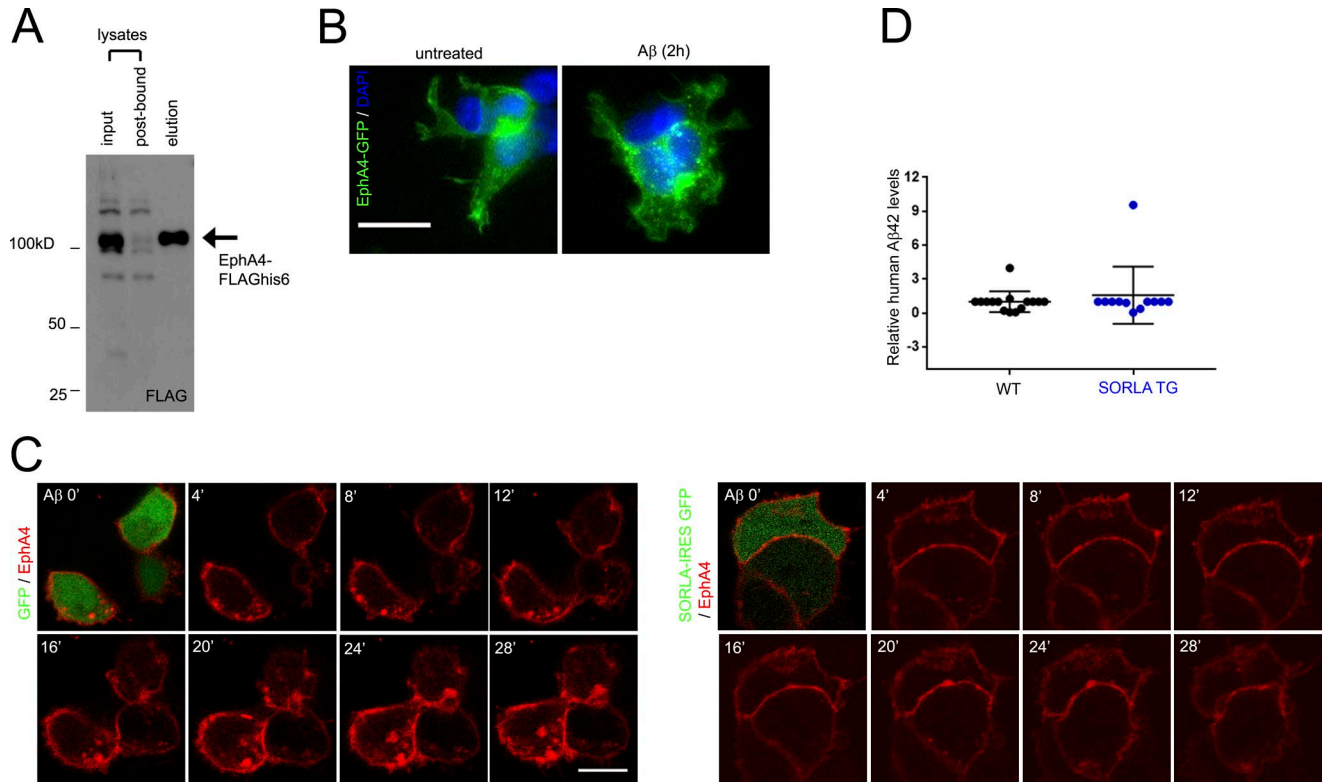


Figure S1. **SORLA affects EphA4 activation.** (A) Screening of Eph receptor immunoprecipitates for SORLA interaction. WT mouse brain lysates were coimmunoprecipitated with control antibodies or EphB1, EphA4, or EphB2, and immunoprecipitates were immunoblotted for SORLA. Dashed line indicates non-adjacent lanes in the blot. (B) SORLA interacts with the EphA4 ectodomain. Control or EphA4-Fc immobilized on protein G Sepharose was incubated with cell lysates overexpressing SORLA, and coprecipitation of SORLA was detected by immunoblot. (C) SORLA is not an EphA4 substrate. Vector control, WT, or a K563R kinase dead EphA4 mutant constructs were transfected into HEK293T cells. Lysates were immunoblotted for EphA4 (left) or immunoprecipitated with control, SORLA, or EphA4 antibodies, and immunoprecipitates were immunoblotted for phosphotyrosine (right). Blots from the immunoprecipitates were then reprobbed with SORLA or EphA4 antibodies (bottom). (D and E) EphrinA1 stimulation results in prolonged EphA4 activation. HEK293 cells stably expressing EphA4 (D) or primary cortical neurons (E) were incubated with ephrinA1-Fc or Fc control for the time indicated, EphA4 was immunoprecipitated from lysates, and the immunoprecipitates were probed for pY602 or EphA4. (F) Steady-state EphA4 activation levels are comparable between control and SORLA TG neurons. pY602/EphA4 ratios in EphA4 immunoprecipitates from WT and SORLA TG (TG) cortical neurons were measured without ephrinA1-Fc stimulation (mean ± SE from four independent experiments). (G) EphA4 activation is enhanced in SORLA KO neurons. WT and SORLA KO neurons were stimulated with ephrinA1-Fc (A1-Fc) for the time indicated, and EphA4 was immunoprecipitated from neuronal lysates and immunoblotted for pY602 or EphA4. Graph represents mean ± SE from three independent experiments ( $n = 3$ ; \*,  $P < 0.005$ ; Student's  $t$  test).



**Figure S2. Steady-state EphA4 cell surface levels are not affected by SORLA, and total/membrane-associated EphA4 levels are similar with SORLA overexpression in neurons and SORLA TG mice.** (A) SORLA overexpression does not affect the levels of EphA4 on the cell surface. HEK293T cells transfected with control/SORLA overexpression vectors (top) or WT/SORLA TG cortical neurons (bottom) were subjected to cell-surface biotinylation, and labeled proteins were precipitated with streptavidin agarose and immunoblotted for EphA4. (B) SORLA depletion or KO does not affect surface EphA4 levels. HEK293T cells transfected with control or SORLA siRNA oligonucleotides (top) or WT/SORLA KO cortical neurons (bottom) were subjected to cell-surface biotinylation as in A, and surface EphA4 levels were examined by immunoblotting. In A and B, top graphs represent (from HEK experiments) mean  $\pm$  SE from three replicates, and bottom graphs (from cortical neurons) represent six replicates from two independent experiments. (C) Total EphA4 levels are unaffected in SORLA TG neurons. EphA4 levels were determined in cultured WT and SORLA TG cortical neurons by immunoblotting, and EphA4/actin ratios normalized to WT neurons were plotted (mean  $\pm$  SE; plots are from nine individual replicate cultures in three independent experiments). (D) Hippocampal tissue from a WT mouse was subjected to biochemical membrane separation to separate synaptosomes and presynaptic and postsynaptic enriched protein components. Equal protein quantities were loaded and immunoblotted for the components indicated. (E) Hippocampal tissue from WT and SORLA TG mice were collected at 3 and 6 mo and subjected to fractionation for Triton X-100-soluble (TX-soluble) membranes and PSD-enriched fractions. Relative EphA4 values normalized to synaptophysin (SVP38) and PSD95 were plotted normalized to WT values (set to 1.0; mean  $\pm$  SE from four age-/litter-matched animals of each age/genotype/fraction).



**Figure S3. EphA4 purification and clustering.** (A) A vector expressing EphA4-FLAGhis6 was transfected into HEK293T cells, and cell lysates were incubated with Ni-NTA agarose. Equal volumes of the lysate input before and after (post-bound) Ni-NTA binding and eluates in 0.3 M imidazole were immunoblotted for FLAG. (B) HEK293T cells were transfected with constructs expressing EphA4-GFP (green) and incubated with 500 nM Aβ for 2 h. Bar, 10 μm. (C) SORLA attenuates Aβ-dependent EphA4 clustering. HEK293T cells were cotransfected with vectors expressing EphA4-mCherry (red) and GFP (left) or SORLA-IRES-GFP (right) and exposed to 500 nM Aβ. Images were acquired by confocal live-cell imaging immediately at time 0 and continuously captured at the time points indicated. Bar, 10 μm. (D) SORLA overexpression has no effect on Aβ clearance or catabolism in vivo. Hippocampal tissue from Aβ<sub>1-42</sub>-injected WT and SORLA TG mice subjected to Morris water maze analysis were subjected to Aβ<sub>1-42</sub> extraction and analysis using an ELISA system for human Aβ<sub>1-42</sub>. Relative Aβ<sub>1-42</sub> levels were normalized to WT Aβ<sub>1-42</sub> (set to 1.0;  $n = 15$  WT and  $n = 12$  SORLA TG animals); graph represents mean  $\pm$  SD.

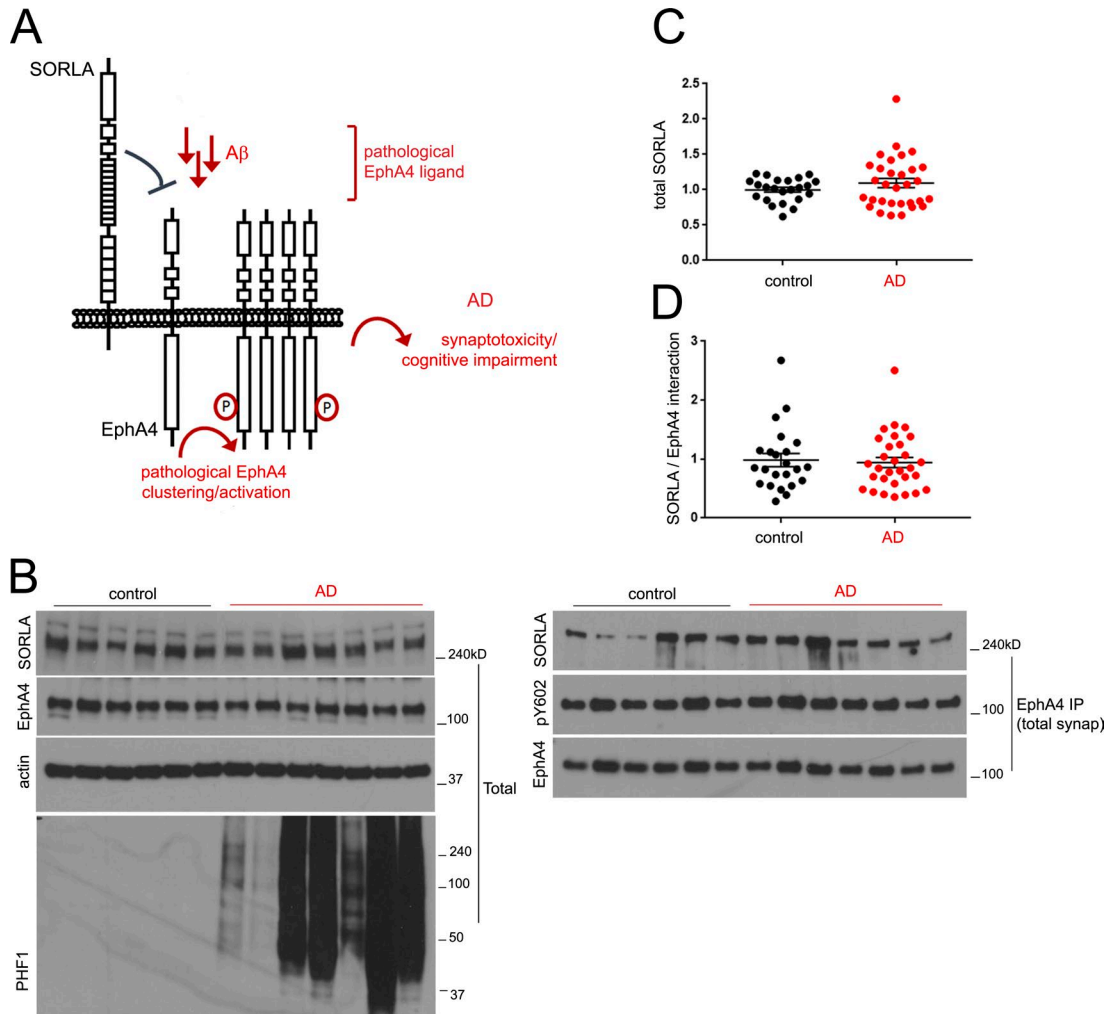


Figure S4. **Variability in total SORLA levels and association with EphA4 in control and AD populations.** (A) A model for SORLA-mediated attenuation of EphA4 activation in response to A $\beta$ . SORLA and EphA4 interact, which attenuates EphA4 clustering and activation in response to A $\beta$  (red), which attenuates downstream synaptotoxic effects in AD. (B–D) Testing the model for SORLA/EphA4 interaction in human AD. (B) Immunoblot of total brain tissue lysates and EphA4 immunoprecipitates from total synaptosomes isolated from representative control and AD patient cohorts. (C) SORLA levels from total brain lysates in control and AD brain. (D) SORLA/EphA4 ratios in EphA4 immunoprecipitates derived from control and AD brain. Graphs in C and D indicate individual data points; mean  $\pm$  SE (control,  $n = 23$ ; AD,  $n = 30$ ).

Table S1. List of human brain tissues used

Number	Source	Identifier	Diagnosis	Sex	Age yr	Braak stage
1	UCSD	X5709	Normal	M	94	2
2	UCSD	X5628	Normal	F	80	1
3	UCSD	X5248	Normal	F	93	1
4	UCSD	X5114	Normal	M	87	1.1
5	UCSD	X5070	Normal	F	97	1
6	UCSD	X5049	Normal	F	102	1
7	UCSD	X4996	Normal	M	91	3
8	UCSD	X4954	Normal	M	76	0
9	UCSD	X5732	AD	F	78	6.2
10	UCSD	X5725	AD	F	66	6.2
11	UCSD	X5720	AD	F	77	6.2
12	UCSD	X5707	AD	M	82	6.2
13	UCSD	X5704	AD	M	77	6.2
14	UCSD	X5698	AD	F	77	6.2
15	UCSD	X5693	AD	F	78	6.2
16	UCSD	X5691	AD	F	62	6.2
17	UCSD	X5689	AD	F	74	6.2
18	UCSD	X5686	AD	M	88	6.2
19	UCSD	X5685	AD	F	88	6.2
20	UCSD	X5684	AD	M	68	6.2
21	UCSD	X5680	AD	M	84	6.2
22	UCSD	X5302	Normal	F	83	1.1
23	UCSD	X5130	Normal	M	71	1
24	UCSD	X5006	Normal	M	69	0
25	UCSD	X4942	Normal	M	83	0
26	UCSD	X4689	Normal	F	79	0
27	UCSD	X5754	AD	M	92	6.2
28	UCSD	X5743	AD	M	87	6.2
29	UCSD	X5738	AD	F	85	6.2
30	UCSD	X5667	AD	F	71	6.2
31	UCSD	X5658	AD	F	70	6.2
32 <sup>a</sup>	UMiami	HCTZZA_16_009	Normal	M	89	
33	UMiami	HCTZZC_16_009	Normal	F	82	
34	UMiami	HCTZZH_16_010	Normal	F	65	
35	UMiami	HCTZZV_16_001	Normal	F	86	
36	UMiami	HBDE16_16_03	Normal	M	83	
37	UMiami	HCTZZR_16_006	AD	M	86	III–IV
38	UMiami	HBCG_16_003	AD	F	90	III–IV
39	UMiami	HBED_16_004	AD	F	71	III–IV
40	UMiami	HBEK_16_001	AD	F	77	V–VI
41	UMiami	HBFF_16_004	AD	M	85	III–IV
42	UMiami	HBFP_16_001	AD	F	83	V–VI
43	UMiami	HBFR_16_001	AD	F	69	V–VI
44	UMiami	HCTYH_16_013	Normal	F	71	
45	UMiami	HCTYP_16_019	Normal	M	75	
46	UMiami	HCTYY_16_006	Normal	M	90	
47	UMiami	HCTZL_16_005	Normal	F	65	
48	UMiami	HCT15HAB16_016	Normal	M	67	
49	UMiami	HCTZT_16_006	Normal	M	76	
50	UMiami	HCTYN_16_001	AD	F	80	V–VI
51	UMiami	HCTZX_16_001	AD	M	95	V–VI
52	UMiami	HCTZZF_16_004	AD	F	103	III–IV
53	UMiami	HBBX_16_001	AD	F	94	V–VI
54	UMiami	HBDA_16_001	AD	M	80	V–VI
55	UMiami	HBDM_16_001	AD	M	60	V–VI
56	UMiami	HBEC_16_001	AD	M	71	V–VI

UCSD, University of California, San Diego; UMiami, University of Miami.

<sup>a</sup>32–43 are samples (in order, left to right) in Fig. 7; 44–56 are samples in Fig. S4.